



Assessment of water security under climate change for the large watershed of Dorudzan Dam in southern Iran

Mostafa Naderi^{1,2}

Received: 19 September 2019 / Accepted: 1 April 2020 / Published online: 23 April 2020
© Springer-Verlag GmbH Germany, part of Springer Nature 2020

Abstract

‘Blue water’ is the portion of freshwater flowing through rivers and the subsurface (groundwater) that is available for human consumption. ‘Green water’ is the portion stored in the unsaturated soil and vegetation canopy that is available only indirectly. Security of blue and green water resources is assessed over the Dorudzan Dam watershed in southern Iran. Precipitation and temperature data from 22 models of the Coupled Model Intercomparison Project Phase 5 are transiently downscaled at five climatic stations under three Representative Concentration Pathway (RCP) scenarios. The Soil and Water Assessment Tool (SWAT) is used to simulate and quantify blue and green water components over the region at the present time and under climate-change conditions. Climate-change study indicates that precipitation decreases (13–17%) and temperature increases (1.7–3.3 °C) under the three RCPs, leading to substantial dam-inflow reduction. Evapotranspiration will increase while soil-water content will decrease, further intensifying green-water scarcity and vulnerability. Water use from the Kor River is sustainable at present, but future climate change will raise some ecological hotspots. Groundwater exploitation is currently unsustainable in all aquifers of the study area and climate change will further decrease the available groundwater, leading to intensification of the water crisis. Assessment of inter-annual security under climate change indicates that maximum scarcities of green water and surface blue water occur during spring and summer, and subsurface blue water (groundwater) maxima occur throughout the year. Thus, climate change threatens the future security of water resources in this arid watershed, requiring different management strategies for sustainability.

Keywords Water security · Climate change · CMIP5 models · Arid regions · Iran

Introduction

Environmental and human water security may decrease due to uncertainties in the future climate, population growth, water demand and changes in social welfare and human lifestyle (Rodrigues et al. 2014). Precipitation, the main source for freshwater supply (Mishra and Singh 2010), may be reduced due to climate change, resulting in limited available water in the future. The available freshwater is classified into ‘blue’ and ‘green’ water resources. Blue water is the portion of

freshwater flowing through the surface (rivers) and subsurface (groundwater) media that can be directly used for human consumption (Hoekstra et al. 2011; Rodrigues et al. 2014). Green water is defined as the portion of freshwater stored in the unsaturated soil layer and vegetation canopy that is available for human use only indirectly (Falkenmark and Rockström 2006; Rodrigues et al. 2014). The security of blue and green water resources is assessed using concepts of water scarcity and vulnerability, which are useful tools applied for sustainable water management and development (Hoekstra et al. 2011). Blue water scarcity is the ratio of water abstraction to available water, while the vulnerability is the ratio of water abstraction to low volume (30th percentile) of available water. Low volume of available water is the historical water availability with a cumulative probability of 0.3; therefore, available water exceeds low volume of available water during 70% of the study period (Gleeson and Wada 2013; Veetil and Mishra 2016). Green water scarcity is the ratio of actual evapotranspiration to available soil-water content, while the

✉ Mostafa Naderi
m.naderi@iasbs.ac.ir; naderi64@gmail.com

¹ Department of Earth Sciences, Institute for Advanced Studies in Basic Sciences (IASBS), Zanjan 45137-66731, Iran

² Research Center for Basic Sciences and Modern Technologies (RBST), Institute for Advanced Studies in Basic Sciences (IASBS), Zanjan 45137-66731, Iran

vulnerability is the ratio of actual evapotranspiration to low volume (30th percentile) of available soil-water content (Veettil and Mishra 2016). Scarcity values can be used to interpret the sustainable water resources management and planning strategies in a given region. When the scarcity value is zero, water resources are fully safe and secure (natural condition) because water is not abstracted from the water resources. Values between zero and 1 indicate that a portion of available water, depending on the scarcity value, is consumed but the region's water resource is not under water stress. A scarcity value of 1 shows that all available water is consumed and there is no capacity for further abstraction. Values greater than 1 imply water resource is under mismanagement, where an abstraction rate greater than the available water makes the region water-stressed; therefore, water abstraction must be reduced in such regions to achieve sustainable development and management. Vulnerability shows value of scarcity, with the same interpretation, during droughts when the available water for consumption is lower than that in normal or wet periods; thus, the vulnerability value can be applied for sustainable development of water resources during droughts in a given region. Spatial and temporal analysis of the water footprint and availability can help to find regions that are under water stress (water footprint > water availability). These regions are referred to as "ecological hotspots" in the literature (Gleeson and Wada 2013; Rodrigues et al. 2014; Veettil and Mishra 2016). Water footprint analysis is a useful concept applied to sustainable development interpretations, but the estimated long-term footprint has an uncertainty due to climate change, even with the assumption of no increase in water demand. It seems that climate change must be incorporated in water-footprint analysis to make more reliable interpretations for sustainable management and development in the future (Papadopoulou et al. 2016; Zhang et al. 2015).

The climate in southern Iran predominantly varies from arid to semi-arid. The occurrences of severe droughts and increased abstraction rates from water resources in recent decades have led to increased water shortage (Iranian Water Resources Management Company 2016); however, climate change may intensify water crisis in southern Iran and make water management difficult in the future. Dorudzan Dam is located in southern Iran, where the main issues in sustainable management of the dam watershed are to quantify future available water and increased water demand under climate change. In this study, future water demand under climate change is assumed to be constant and equal to the baseline demand. This assumption allows one to assess only the impact of climate change on the security of blue and green water resources over the region; therefore, the objective of this study is to assess the availability and vulnerability of blue and green water resources over the large watershed of Dorudzan Dam under climate change with assumption of no increase in future water demand.

Study area

The study area, with a predominantly arid to semi-arid climate, is located in northern Fars Province of southern Iran (Fig. 1). Multi-purpose Dorudzan Dam, with a 4,304 km² watershed, was constructed on the Kor River in the year 1972 to generate electrical power, control flooding and supply irrigation water requirement for downstream areas (1,100 km²) and municipal-industrial water requirement for three cities: Shiraz, Marvdasht and Zarghan. An upstream dam, Mollasadra, was constructed in the watershed of the Dorudzan Dam (Fig. 1) and has operated since August 2007. The upstream cultivated area (Fig. 1) is about 1,076 km², where river water and groundwater from the three aquifers Aspas, Khosroshirin and Kamfiruz are exploited to supply the irrigation water requirement. Groundwater storage has been depleted in these three aquifers during the last two decades due to overexploitation and severe droughts (Iranian Water Resources Management Company 2016). Pasture (PAST) and forest (FRST) is spread over an area of 3,185 km² covering 74% of the watershed (Fig. 1). Daily river flow is measured at nine hydrometric stations within the study area. Daily data at four stations have been measured since 1997 and at one station since 2009; these stations are not located on the main river. However, daily river flow has also been measured at four hydrometric stations (Dehkadeh Sefid (Sefid), Dehkadeh Sefid (Gavgodar), Chameriz and Dorudzan) since 1978, of which three are located on the main river (Fig. 1); therefore, measured daily discharges at these four stations are used in this study due to available long-period recorded data. Mean annual discharges at hydrometric stations of Dehkadeh Sefid (Sefid), Dehkadeh Sefid (Gavgodar), Chameriz and Dorudzan Dam were 4.43, 6.5, 25.4 and 28.6 m³/s, respectively, during the period 1978–2015. Mean annual inflow and outflow of the Mollasadra Dam were 6.2 and 7 m³/s, respectively, during the dam operation period of 2007–2015. Mean annual precipitation ranged from 677 to 820 mm over the watershed, while it increased up to 855 mm in western regions. Mean annual precipitation over the watershed of Dorudzan Dam was 751 mm during the observation period 1978–2015.

Methodology

Climate change study

In this study, daily temperature and precipitation data from 22 general circulation models (GCMs) of the Coupled Model Inter-comparison Project Phase 5 (CMIP5) were used to study climate change during the period 2026–2085 under three representative concentration pathway (RCP) scenarios. The RCPs include a stringent mitigation scenario of RCP2.6, an intermediate scenario of RCP4.5 and a very high greenhouse

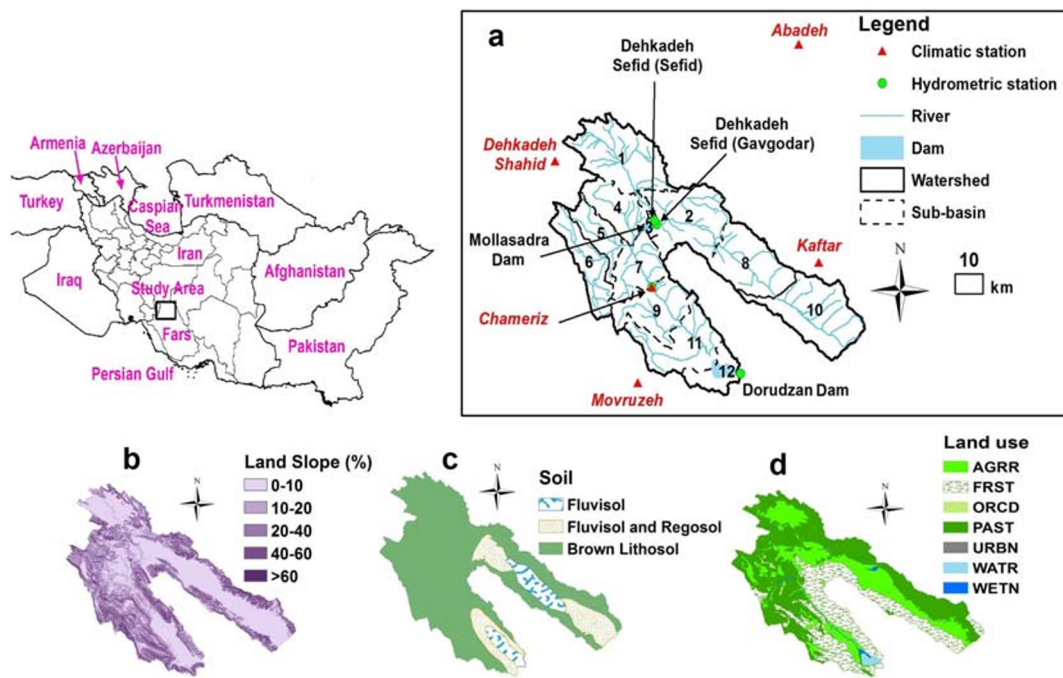


Fig. 1 a The study area and spatial distribution of **b** land slope, **c** soil data and **d** land use. Land use consists of agriculture (AGRR), forest (FRST), orchard (ORCD), pasture (PAST), urban (URBN), water body (WATR) and wetland (WETN)

gasses emission scenario of RCP8.5. CMIP5 models also provide daily outputs for RCP6.5, but this scenario was not included in this climate change study, because RCP6.5 shows a level of warming between scenarios RCP4.5 and RCP8.5. The uncertainty associated with occurrence of a scenario in the future reveals that climate change would be assessed under the best (RCP2.6), intermediate (RCP4.5) and worst (RCP8.5) cases to include all possible trajectories (Lutz et al. 2016); therefore, in this research, climate change was studied under the three scenarios of RCP2.6 (best), RCP4.5 (intermediate) and RCP8.5 (worst).

The CMIP5 provides outputs of more than one GCM from an individual institution or more than one version of a given GCM (Ho et al. 2016; Thompson et al. 2017), leading to model-dependent and institution-dependent results for climate change studies (Ho et al. 2016; Knutti and Sedláček 2013; Thompson et al. 2017). Potential for such biases to influence the ensemble mean can be addressed using the climate sensitivity indices approach (Naderi and Saatsaz 2019; Semenov and Stratonovitch 2015).

The available number of GCMs, regardless of version and institution, were 16, 31 and 30 models for the RCP2.6, RCP4.5 and RCP 8.5, respectively (Table 1). The method of climate sensitivity indices (CSI) proposed by Semenov and Stratonovitch (2015) was used to select a subset of GCMs, while it preserves the range of uncertainty that exists in the CMIP5 models and eliminates model-dependent biases. The CSI for precipitation (temperature) is defined as the spatial-averaged, calculated over a region, relative change

(difference) between mean values for the future and baseline periods of a given GCM. Then, the 25th (limit of lowest values) and 75th (limit of highest values) CSI percentiles were selected to include GCMs in the climate change study (Fig. 2; Table 1; Naderi and Saatsaz 2019). Included GCMs are 12, 21, and 22 models for the RCP2.6, RCP4.5, and RCP 8.5, respectively (Fig. 2; Table 1).

GCMs predict precipitation and temperature of a grid box at coarse resolutions (at least 250 km); however, data would be required at a local level to analyze the impact of climate change on rivers watersheds (Chen et al. 2011). Therefore, GCM outputs must be downscaled (finer spatial resolution) to each climatic station inside the watershed. A stochastic weather generator, Long Ashton Research Station Weather Generator (LARS-WG), was used to downscale daily precipitation and temperature data from each GCM to five climatic stations in the study area, making finer spatial resolutions of the GCM outputs across the watershed. The climatic stations are Abadeh, Kaftar, Dehkadeh Shahid, Chameriz and Movruzeh (Fig. 1). Daily precipitation was measured at five stations during the period 1978–2015, but the record of daily minimum and maximum temperature was limited to the Abadeh synoptic station. Observed daily data at five climatic stations during the period 1978–2005 are inputted to the LARS-WG for calibration. Then, the LARS-WG is verified by comparison between generated and observed precipitation and temperature data in which monthly statistical distributions and mean monthly values are compared (Fig. 3) using the Kolmogorov–Smirnov and Student's *t*-test, respectively, at

Table 1 Available, included (*italic*) and excluded (non-*italic*) general circulation models (GCMs) for the study area under the three RCPs

GCM number	RCP2.6	RCP4.5	RCP8.5
1	–	<i>ACCESS1.0</i>	<i>ACCESS1.0</i>
2	–	<i>ACCESS1.3</i>	<i>ACCESS1.3</i>
3	–	<i>CCSM4</i>	<i>CCSM4</i>
4	–	–	<i>CMCC-CESM</i>
5	–	<i>CMCC-CM</i>	<i>CMCC-CM</i>
6	–	<i>CMCC-CMS</i>	<i>CMCC-CMS</i>
7	<i>CNRM-CM5</i>	<i>CNRM-CM5</i>	<i>CNRM-CM5</i>
8	<i>CSIRO-Mk3.6.0</i>	<i>CSIRO-Mk3.6.0</i>	<i>CSIRO-Mk3.6.0</i>
9	–	CSIRO-Mk3L-1-2	–
10	–	EC-EARTH	EC-EARTH
11	FGOALS-g2	FGOALS-g2	FGOALS-g2
12	–	FGOALS-s2	FGOALS-s2
13	GFDL-CM3	GFDL-CM3	GFDL-CM3
14	GFDL-ESM2G	GFDL-ESM2G	GFDL-ESM2G
15	–	<i>GISS-E2-H</i>	<i>GISS-E2-H</i>
16	–	<i>GISS-E2-R</i>	<i>GISS-E2-R</i>
17	–	HadCM3	–
18	<i>HadGEM2-AO</i>	<i>HadGEM2-AO</i>	<i>HadGEM2-AO</i>
19	–	HadGEM2-CC	HadGEM2-CC
20	<i>HadGEM2-ES</i>	<i>HadGEM2-ES</i>	<i>HadGEM2-ES</i>
21	–	<i>INM-CM4</i>	<i>INM-CM4</i>
22	<i>IPSL-CM5A-LR</i>	<i>IPSL-CM5A-LR</i>	<i>IPSL-CM5A-LR</i>
23	<i>IPSL-CM5A-MR</i>	<i>IPSL-CM5A-MR</i>	<i>IPSL-CM5A-MR</i>
24	–	<i>IPSL-CM5B-LR</i>	<i>IPSL-CM5B-LR</i>
25	<i>MIROC-ESM</i>	<i>MIROC-ESM</i>	<i>MIROC-ESM</i>
26	<i>MIROC-ESM-CHEM</i>	<i>MIROC-ESM-CHEM</i>	<i>MIROC-ESM-CHEM</i>
27	–	MIROC4h	–
28	MIROC5	MIROC5	MIROC5
29	<i>MPI-ESM-LR</i>	<i>MPI-ESM-LR</i>	<i>MPI-ESM-LR</i>
30	<i>MPI-ESM-MR</i>	<i>MPI-ESM-MR</i>	<i>MPI-ESM-MR</i>
31	<i>MRI-CGCM3</i>	<i>MRI-CGCM3</i>	<i>MRI-CGCM3</i>
32	–	–	MRI-ESM1
33	<i>Nor-ESM1-M</i>	<i>Nor-ESM1-M</i>	<i>Nor-ESM1-M</i>
No. of included models	12	21	22
No. of excluded models	4	10	8

the significance level of 0.01 (Iizumi et al. 2012; Semenov and Barrow 2002). All tests are accepted in five stations at this significance level. In the final step, change factors, calculated from daily data of each GCM, are applied by LARS-WG to downscale daily precipitation, and minimum and maximum temperature at five stations (Semenov and Barrow 2002). Change factors for precipitation amount, wet and dry series, and standard deviation of the mean temperature are defined as the ratio of corresponding values in the future period (selected time window) to baseline period values (calibration period). The minimum and maximum temperature change factors are the difference between corresponding values of the future and baseline periods (Semenov and Barrow 2002). In this study,

change factors for each GCM data and each year during the period 2026–2085 were transiently calculated via a 1-year forward shifting procedure in which future time windows were selected as 5-year (Naderi and Raeisi 2016); therefore, daily precipitation and temperature data from each CMIP5 model were downscaled to five climatic stations under the RCP2.6, RCP4.5 and RCP8.5 (2026–2085).

Hydrologic modeling

The physically based semi-distributed hydrological model of Soil and Water Assessment Tool (SWAT; Abbaspour et al. 2009) was used to quantify blue and green water resources

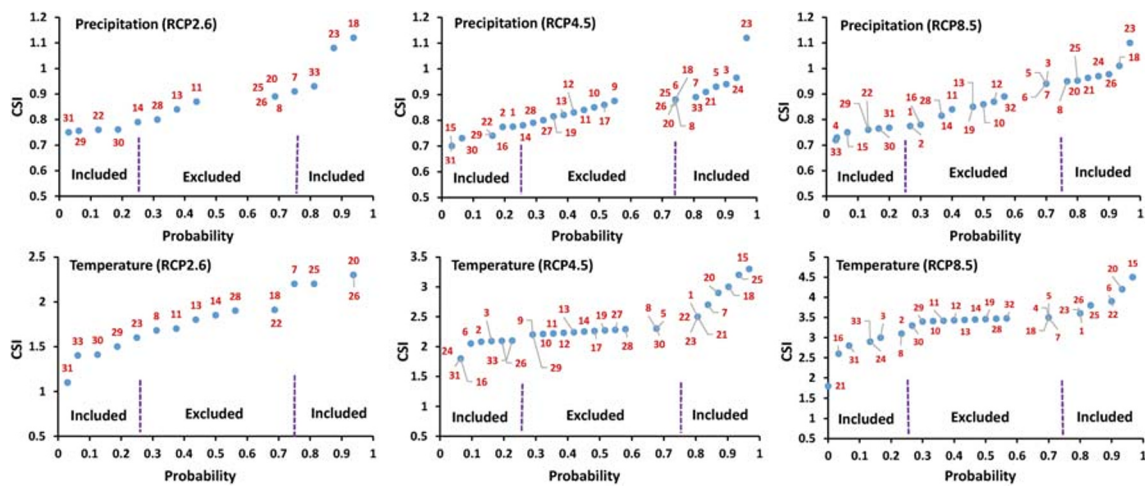
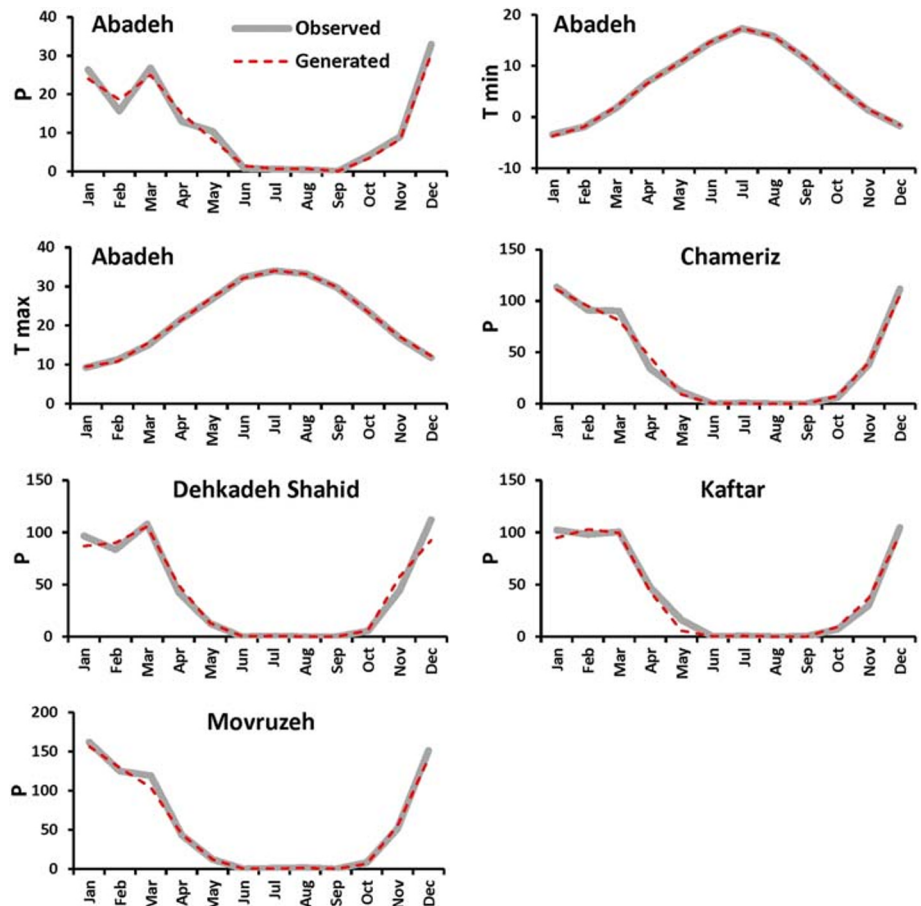


Fig. 2 Probability distribution of precipitation and temperature climate sensitivity indices (CSI) values for available CMIP5 models over the watershed of Dorudzan Dam. Numbers denote the related number of the general circulation models (GCM) listed in Table 1

in the study area. Model inputs are data on topography, land use, soil and climate. The observation period (1978–2015) is classified into 28-year calibration (1978–2005) and 10-year validation (2006–2015) periods. The first 3 years of the calibration period (1978–1980) is selected for the SWAT warm-up.

The ArcSWAT 2012 interface was used to setup and parameterize the hydrological model. The dam watershed was delineated using 30-m digital elevation modeling, and it was further divided into 12 subbasins (Fig. 1). Land use (Fig. 1) consists of pasture (43.44%), forest (30.65%), agriculture (23.87%), wetland (0.8%), water body (0.75%), orchard

Fig. 3 Comparison between observed and generated values of mean monthly minimum (Tmin) and maximum (Tmax) temperature and precipitation (P) for five climatic stations



(0.29%) and urban areas (0.2%)—Iranian Water Resources Management Company (2016). The watershed was classified into five slope ranges of 0–10, 10–20, 20–40, 40–60 and >60% (Fig. 1). Ten elevation bands were defined in each subbasin to capture the precipitation lapse rate well. The soil (see Fig. 1) contains brown Lithosols (76.9%), Fluvisols-Regosols (16.1%) and Fluvisols (7%) over the study area (FAO/IIASA/ISRIC/ISSCAS/JRC 2009; Iranian Water Resources Management Company 2016). The dam watershed was classified into 301 hydrological response units (HRUs) by defined thresholds of 5, 5 and 1% for land use, soil and slope data, respectively. Land use threshold is used by the SWAT to eliminate minor land uses in each subbasin. Land uses that cover a percentage of the subbasin area less than the threshold level are eliminated. After the elimination process, the area of the remaining land uses is reapportioned so that 100% of the land area in the subbasin is modeled. The SWAT model uses the same process for soil and slope data (Winchell et al. 2013). The daily precipitation data of five climatic stations, the nearest station for each HRU, are used by the SWAT to capture the spatial variation of precipitation. Potential evapotranspiration and surface runoff were calculated using methods of the Hargreaves and SCS curve number, respectively. Daily outflow of the Mollasadra Dam during the operation period (2007–2015) was included in the SWAT. Monthly abstraction rates from river water and groundwater were inputted to the SWAT for each subbasin (Table 2) based on the reference data at year 2009 (Iranian Water Resources Management Company 2016). The abstraction rates increase during summer and reduce during winter through the subbasins.

The daily Kor River flow was measured at hydrometric stations Dehkadeh Sefid (Sefid), Dehkadeh Sefid (Gavgodar), Chameriz and Dorudzan Dam (Fig. 1) during the period 1978–2015. When the model is calibrated and validated, downscaled precipitation and temperature at five climatic stations under the three RCPs were included in the SWAT to predict daily discharges under climate change.

The algorithm of Sequential Uncertainty Fitting version 2 (SUFI-2), incorporated in the SWAT Calibration and Uncertainty Program (SWAT-CUP), was used for calibration, validation and sensitivity analysis (Abbaspour et al. 2009). The SUFI-2 incorporates all uncertainties associated with input data and model parameters and predicts the output quantified by 95% prediction uncertainty (95PPU). The model performance was evaluated using goodness-of-fit criteria of the coefficient of determination (R^2), Nash-Sutcliffe (NS), P- and R-factor. P-factor is the percentage bracketing of measured data within prediction uncertainty, but R-factor is the ratio of average width of the 95PPU band to the standard deviation of observed data (Abbaspour et al. 2009). The dynamic baseflow method was used by SUFI-2 in which the daily baseflow was determined at four hydrometric stations using the automated baseflow separation program PART. Program PART is

developed based on the methodology proposed by Knisel and Sheridan (1983) and Shirmohammadi et al. (1984)—further details can be found in Linsley Jr. et al. (1975) and Rutledge (2007).

The SWAT calibrated parameters are the curve number 2 (CN2), soil hydraulic conductivity (SOL-K), soil available water content (SOL-AWC), overland flow Manning's roughness (OV-N), groundwater delay (GW-DELAY), threshold depth of water in the shallow aquifer required for baseflow to occur (GW-QMN), baseflow alpha factor (ALPHA-BF), groundwater reevaporation coefficient, (GW-REVAP), threshold depth of water in the shallow aquifer for evaporation to occur (REVAP-MN), soil evaporation compensation factor (ESCO) and deep-aquifer percolation fraction (RCHRG-DP). The SUFI-2 algorithm in the SWAT-CUP interface allows for parameter sensitivity analysis. Sensitivity of the parameters is assessed using the Student's t-test (t-stat) and P -values in which more sensitive parameters have larger t-stat absolute values and smaller P -values (Abbaspour et al. 2009).

Blue and green waters security assessment

The HRU output in SWAT provides sufficient data to quantify blue and green waters. Green water is the sum of actual evapotranspiration (ET) and soil-water content (SW) (Abbaspour et al. 2009; Veetil and Mishra 2016). Blue water is the sum of the amount of water leaving the HRU and entering the main channel (WYLD) and groundwater storage. Groundwater storage (renewable groundwater) is defined as the difference between total recharge to aquifers (GW-RCHG) and baseflow (GW-W) (Veetil and Mishra 2016). Security of the freshwater (blue and green) was quantified by two indices: water scarcity and vulnerability.

Green water scarcity and vulnerability

The green water footprint refers to indirect use of freshwater by humans to produce goods and services and it is equal to actual evapotranspiration from an agricultural area (Hoekstra et al. 2011). The green water scarcity and vulnerability are calculated using the following equations (Hoekstra et al. 2011; Veetil and Mishra 2016):

$$GW_{\text{scarcity}(i,t)} = GW_{\text{footprint}(i,t)} / GW_{\text{availability}(i,t)} \quad (1)$$

$$GW_{\text{vulnerability}(i,t)} = GW_{\text{footprint}(i,t)} / GW_{\text{availability}(P30)(i,t)} \quad (2)$$

in which $GW_{\text{footprint}(i,t)}$ is the green water footprint, $GW_{\text{availability}(i,t)}$ the available green water, and $GW_{\text{availability}(P30)(i,t)}$ the historical low availability of green water in subbasin i during time t (month).

The green water footprint and availability are respectively equal to actual evapotranspiration (ET) and initial soil-water

Table 2 Monthly surface-water and groundwater abstraction rates (m³/s) from each subbasin in year 2009

Basin No.	Month											
	Jan	Feb	Mar	Apr	May	Jun	Jul	Aug	Sep	Oct	Nov	Dec
Abstraction rate from Kor River												
1	0	0	0	0.128	0.128	0.128	0.156	0.156	0.156	0.052	0.052	0.052
2	0	0	0	0.125	0.125	0.125	0.152	0.152	0.152	0.072	0.072	0.072
3	0	0	0	0.022	0.022	0.022	0.028	0.028	0.028	0.014	0.014	0.014
4	0	0	0	0.882	0.882	0.882	1.304	1.304	1.304	0.411	0.411	0.411
5	0	0	0	0.057	0.057	0.057	0.088	0.088	0.088	0.026	0.026	0.026
6	0	0	0	0.307	0.307	0.307	0.653	0.653	0.653	0.173	0.173	0.173
7	0	0	0	0.295	0.295	0.295	0.439	0.439	0.439	0.124	0.124	0.124
8	0	0	0	0	0	0	0	0	0	0	0	0
9	0	0	0	2.877	2.877	2.877	5.878	5.878	5.878	1.558	1.558	1.558
10	0	0	0	0	0	0	0	0	0	0	0	0
11	0	0	0	0.817	0.817	0.817	1.864	1.864	1.864	0.329	0.329	0.329
12	0	0	0	0	0	0	0	0	0	0	0	0
Abstraction rate from groundwater												
1	0.002	0.002	0.002	0.218	0.218	0.218	0.334	0.334	0.334	0.118	0.118	0.118
2	0.047	0.047	0.047	2.420	2.420	2.420	3.066	3.066	3.066	0.548	0.548	0.548
3	0	0	0	0	0	0	0	0	0	0	0	0
4	0	0	0	0	0	0	0	0	0	0	0	0
5	0	0	0	0.001	0.001	0.001	0.001	0.001	0.001	0	0	0
6	0.015	0.015	0.015	0.034	0.034	0.034	0.037	0.037	0.037	0.021	0.021	0.021
7	0.001	0.001	0.001	0.031	0.031	0.031	0.092	0.092	0.092	0.020	0.020	0.020
8	0.033	0.033	0.033	5.388	5.388	5.388	6.737	6.737	6.737	1.578	1.578	1.578
9	0	0	0	0.352	0.352	0.352	1.581	1.581	1.581	0.073	0.073	0.073
10	0.009	0.009	0.009	2.034	2.034	2.034	2.413	2.413	2.413	0.727	0.727	0.727
11	0.058	0.058	0.058	1.038	1.038	1.038	3.604	3.604	3.604	0.589	0.589	0.589
12	0	0	0	0.003	0.003	0.003	0.012	0.012	0.012	0.002	0.002	0.002

content (SW_i) in HRU output of the SWAT (Veettil and Mishra 2016; Winchell et al. 2013).

Blue water scarcity and vulnerability

The SWAT HRU output provides the main channel flow (WYLD), total recharge to the aquifer (GW-RCHG) and groundwater contribution to the river flow, i.e., baseflow (GW-Q). In this study, blue water was separately calculated for surface blue water and subsurface blue water. Surface blue water is the amount of water available as river flow (WYLD) (Veettil and Mishra 2016). Subsurface blue water is the groundwater storage, i.e., the groundwater recharge minus groundwater contribution to the river baseflow (Esnault et al. 2014; Gleeson and Wada 2013; Kourgialas et al. 2018). Blue water security was separately quantified for surface and subsurface components using two indices: water scarcity and vulnerability.

Surface blue-water scarcity and vulnerability Surface blue-water scarcity and vulnerability are calculated using the following equations (Hoekstra et al. 2011; Veettil and Mishra 2016):

$$\text{surBW}_{\text{scarcity}(i,t)} = \text{surBW}_{\text{footprint}(i,t)} / \text{surBW}_{\text{availability}(i,t)} \quad (3)$$

$$\begin{aligned} \text{surBW}_{\text{vulnerability}(i,t)} \\ = \text{surBW}_{\text{footprint}(i,t)} / \text{surBW}_{\text{availability}(P30)(i,t)} \end{aligned} \quad (4)$$

in which $\text{surBW}_{\text{footprint}(i,t)}$ is the surface water footprint, $\text{surBW}_{\text{availability}(i,t)}$ the available surface water for consumption, and $\text{surBW}_{\text{availability}(P30)(i,t)}$ the historical low availability of surface water in subbasin i during time t (month).

The surface blue-water footprint is the amount of consumptive water use (Rodrigues et al. 2014; Veettil and Mishra 2016). The $\text{surBW}_{\text{availability}}$ is the amount of water which can be abstracted from a river without affecting river-dependent ecology (Hoekstra et al. 2011; Veettil and Mishra 2016). The

presumptive standard method allows using 20% of the river flow for consumption and leaving 80% for sustaining the environment (Richter et al. 2012).

$$\text{surBW}_{\text{availability}(i,t)} = Q_{(i,t)} - \text{EFR}_{(i,t)} \quad (5)$$

$$\text{EFR}_{(i,t)} = 0.8Q_{\text{mean}(i,t)} \quad (6)$$

where $Q_{(i,t)}$ is the river flow (m^3/s), $\text{EFR}_{(i,t)}$ the environmental flow requirement (m^3/s) and $Q_{\text{mean}(i,t)}$ the long-term mean monthly discharge in subbasin i . The t denotes time in months.

Subsurface blue-water scarcity and vulnerability The groundwater footprint is defined as the required area to sustain groundwater use and groundwater-dependent ecosystem services for the aquifer (Gleeson and Wada 2013).

$$\text{GF} = \left(\frac{C}{R-E} \right) A \quad (7)$$

in which GF is the groundwater footprint, A the aquifer area (m^2) and C , R and E are respectively the area-averaged annual abstraction of groundwater (m^3/s), recharge rate from precipitation and irrigation (m^3/s), and the groundwater contribution to environmental streamflow, i.e., baseflow (m^3/s).

Groundwater stress (GF/A) is a water balance between groundwater abstraction and groundwater available for consumption. The available groundwater ($\text{subBW}_{\text{availability}}$) is defined as the difference between groundwater recharge from precipitation and irrigation (R) and groundwater contribution to stream flow (E) (Esnault et al. 2014; Gleeson and Wada 2013; Kourgialas et al. 2018).

$$\text{subBW}_{\text{availability}} = R - E \quad (8)$$

The historical low availability of groundwater (similar to the definition for surface blue water and green water) can be defined as follows:

$$\text{subBW}_{\text{availability}(P30)} = (R - E)_{(P30)} \quad (9)$$

in which the historical low availability of groundwater is expressed as the 30th percentile of the available groundwater.

Finally, subsurface blue-water scarcity and vulnerability are calculated using the following equations:

$$\begin{aligned} \text{subBW}_{\text{scarcity}(i,t)} \\ = \text{subBW}_{\text{footprint}(i,t)} / \text{subBW}_{\text{availability}(i,t)} \end{aligned} \quad (10)$$

$$\begin{aligned} \text{subBW}_{\text{vulnerability}(i,t)} \\ = \text{subBW}_{\text{footprint}(i,t)} / \text{subBW}_{\text{availability}(P30)(i,t)} \end{aligned} \quad (11)$$

where $\text{subBW}_{\text{footprint}(i,t)}$ is the groundwater abstraction (m^3/s), $\text{subBW}_{\text{availability}(i,t)}$ the available groundwater for consumption (m^3/s), and $\text{subBW}_{\text{availability}(P30)(i,t)}$ the low historical

groundwater availability (m^3/s) in aquifer i during time t (month).

Results and discussion

Precipitation and temperature under climate change

Downscaled annual precipitation data at the five climatic stations under the three RCPs are presented in Fig. 4. The mean annual precipitation varies from 677 to 855 mm over the watershed, resulting in a spatial-averaged value of 751 mm (Fig. 5). Spatial variation of precipitation is not consistent with topography variation because there are greater amounts of precipitation in western and south-western regions at lower altitudes. Precipitation over the region is mainly affected by the Mediterranean (entering the region from north-west) and Red Sea (entering the region from south-west) air masses which generate 74 and 23% of the precipitation, respectively (Alijani and Harman 1985; Beyglou et al. 2009; Roshani et al. 2013). Climate-change study indicates that the spatial ranges of precipitation are 576–770, 495–683 and 529–692 mm under the RCP2.6, RCP4.5 and RCP8.5, respectively (Fig. 5). The spatial-averaged precipitation over the dam watershed will decrease from 751 mm during the observation period to 653, 624 and 630 mm under the RCP2.6, RCP4.5 and RCP8.5, respectively, resulting in percentage reductions by 13, 16.9 and 16.1%, respectively (Fig. 5).

Mediterranean and Red Seas are the main moisture sources for precipitation in southern Iran where their contributions to precipitation are 74 and 23%, respectively (Alijani and Harman 1985; Beyglou et al. 2009; Roshani et al. 2013). The contribution of the Mediterranean air masses will reduce under climate change due to the reduction of cyclogenesis, while the contribution of the Red Sea air masses will increase (Evans 2008; Evans and Alsamawi 2011; Giorgi and Lionello 2008; Mariotti et al. 2008; Ulbrich et al. 2006). Climate change in the study area is substantially influenced by the Mediterranean Sea and, in the second order of importance, by Red Sea, based on their annual contributions in precipitation events; therefore, the resultant impact of climate change on moisture sources of the Mediterranean and Red Seas will lead to precipitation reduction in the future.

Downscaled temperature data from the Abadeh synoptic station show that annual temperature will increase from 15.7 °C in early years of the three RCPs up to 16.2, 17.6 and 19.8 °C in late years of the RCP2.6, RCP4.5 and RCP8.5, respectively (Fig. 5). The mean annual temperature will increase from 14.4 °C during the observation period 1978–2015 to 16.1, 16.7 and 17.7 °C under the RCP2.6, RCP4.5, and RCP8.5, respectively, leading to warming by 1.7, 2.3 and 3.3 °C, respectively.

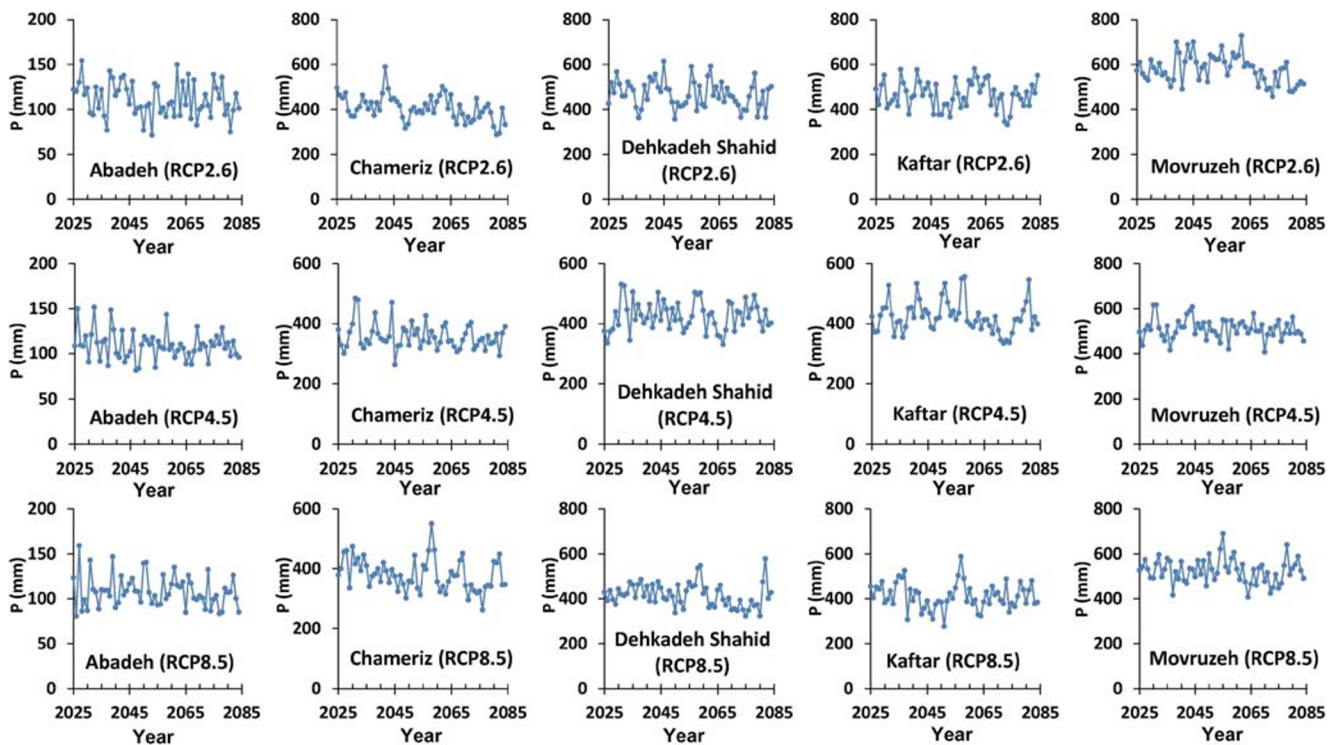


Fig. 4 Downscaled annual precipitation (P) at five climatic stations under the three representative concentration pathway (RCP) scenarios

SWAT evaluation and flow prediction

The mean annual total discharge (baseflow) of the Kor River is 4.43 (3), 6.5 (4.65), 25.4 (18.9) and 28.6 (20.45) m^3/s at hydrometric stations Dehkadeh Sefid (Sefid), Dehkadeh Sefid (Gavgodar), Chameriz and Dorudzan Dam, respectively, during the observation period 1981–2015. Therefore, the dominant discharge of the Kor River originates from groundwater contribution to the stream flow.

The SWAT-predicted daily flow data at four hydrometric stations are compared with observed discharges during the calibration period 1981–2005 (Fig. 6). The ranges of determination coefficient (R^2) and Nash-Sutcliffe (NS) values throughout the hydrometric stations are 0.86–0.92 and 0.73–0.87, respectively. The ranges of P-factor and R-factor are 0.69–0.78 and 0.33–0.53, respectively. The mean annual observed discharges at Dehkadeh Sefid (Sefid), Dehkadeh Sefid (Gavgodar), Chameriz and Dorudzan Dam are 4.6, 6.83, 27.83 and 31.8 m^3/s , respectively, while SWAT-predicted values are 4.58, 6.95, 27.21 and 31 m^3/s , respectively.

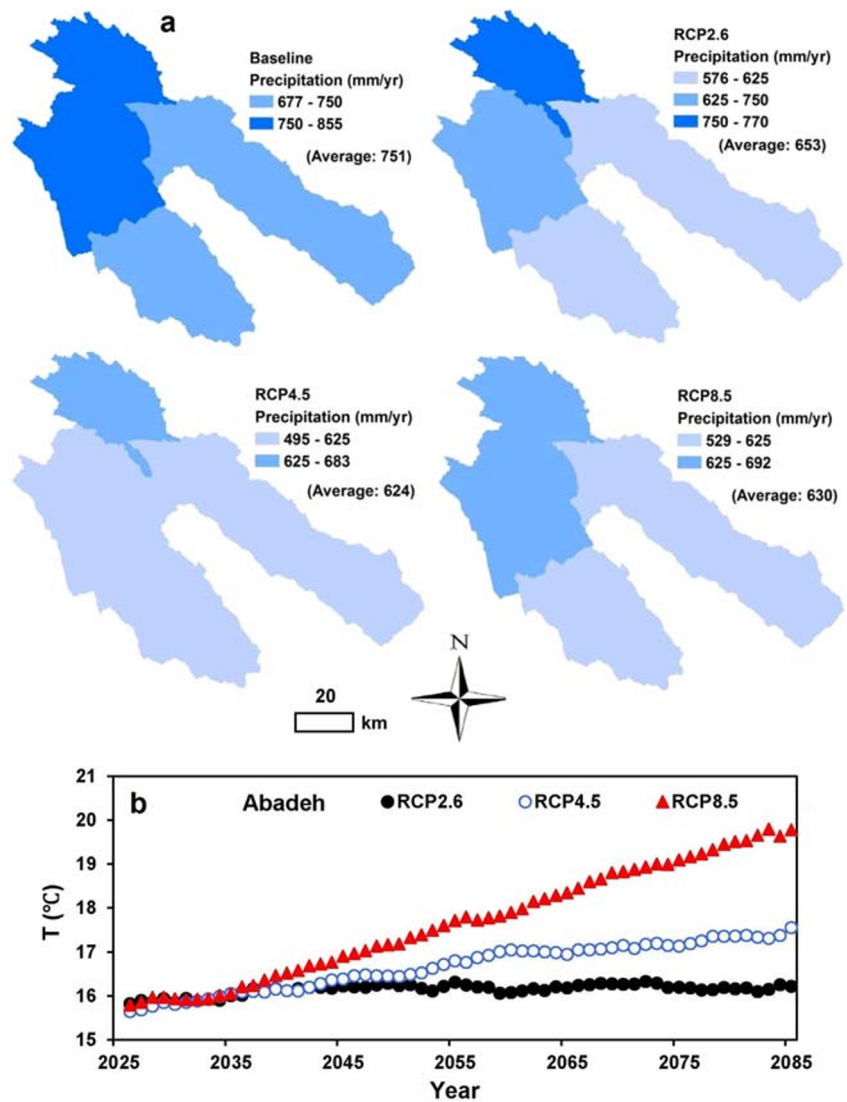
The ranges of R^2 and NS are 0.78–0.9 and 0.75–0.82, respectively during the validation period (2006–2015). Comparison between mean annual observed discharges and predicted discharges during the validation period indicates that the SWAT predicts the corresponding values well. The observed flow at Dehkadeh Sefid (Sefid), Dehkadeh Sefid (Gavgodar), Chameriz and Dorudzan Dam are 3.31, 5, 15.7 and 16.8 m^3/s , respectively, while

corresponding predicted values are 3, 4.97, 15.84 and 17 m^3/s , respectively.

Downscaled daily precipitation and temperature data at five climatic stations are included in the calibrated SWAT to predict daily river flow under climate change. Operation of the Mollasadra dam under climate change is assumed to be similar to that in the observation period. The Mollasadra Dam inflow is the sum of river flow at hydrometric stations Dehkadeh Sefid (Sefid) and Dehkadeh Sefid (Gavgodar). The mean monthly ratio of Mollasadra Dam outflow to inflow is 0.95, 1.74, 0.71, 0.44, 0.84, 1.34, 3, 2.45, 1.76, 0.89, 0.74 and 0.33 for the months of January to December, during the operational period 2007–2015. These monthly ratios are applied to the Mollasadra Dam operation under climate change.

Flow prediction under climate change shows a substantial discharge reduction of the Kor River in the future. The mean annual river flow at Dehkadeh Sefid (Sefid), Dehkadeh Sefid (Gavgodar), Chameriz and Dorudzan Dam will respectively decrease from 4.43, 6.5, 25.4 and 28.6 m^3/s in the present time (1981–2015) to 3.34, 3.7, 17.6 and 14.9 m^3/s , respectively under the RCP2.6 (2026–2085). The corresponding percentage reductions are 24.6, 43, 30.7 and 47.9%, respectively under this scenario. The percentage reductions of river flow at Dehkadeh Sefid (Sefid), Dehkadeh Sefid (Gavgodar), Chameriz and Dorudzan

Fig. 5 **a** Spatial distribution of mean annual precipitation over the watershed during the observation period and three RCPs. **b** Downscaled annual temperature at the Abadeh station under climate change



Dam are 26.4, 44.15, 33.1 and 50%, respectively, under the RCP4.5, and 27.7, 43.8, 32.3 and 49.9%, respectively, under the RCP8.5. The substantial reduction of dam inflow under three RCPs (47.9–50%) is mainly due to the precipitation reduction (13–16.9%), evapotranspiration enhancement (13.6–16%) and reduction of soil-water content (4–15.3%) over the watershed.

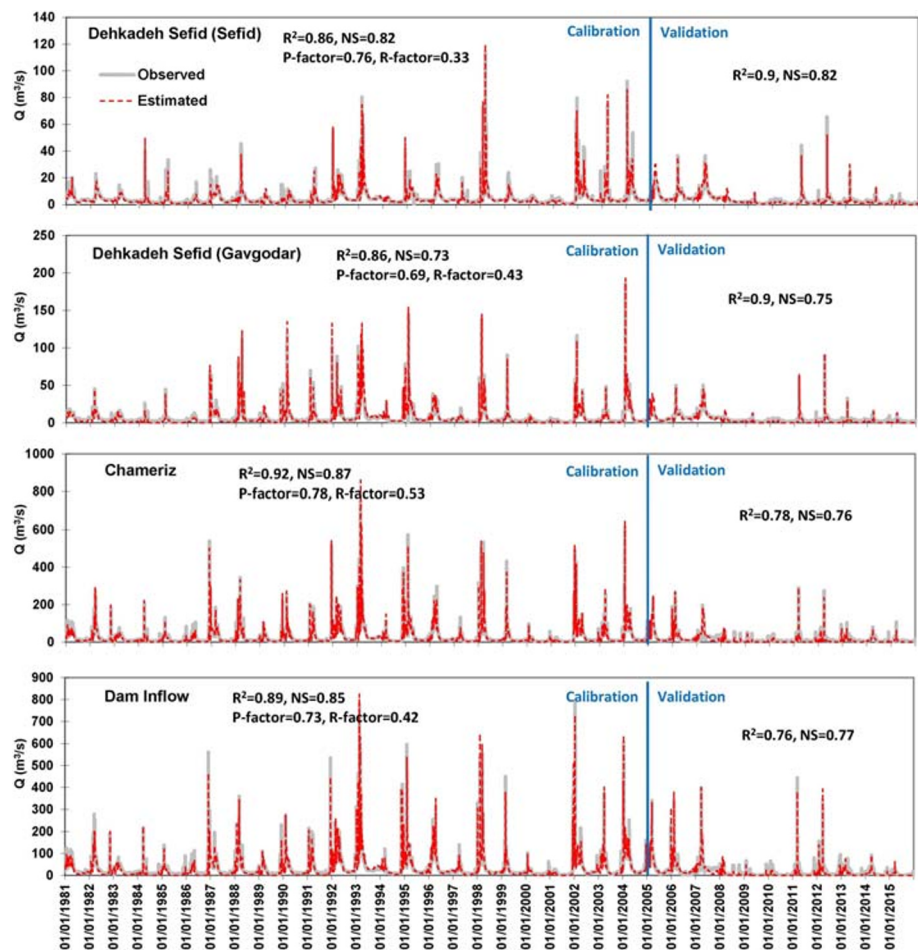
Global sensitivity analysis, which is separately performed for each hydrometric station using the SUF-2 algorithm, indicates that sensitivity of the parameters differs among them. However, the curve number 2 (CN2) and soil hydraulic conductivity (SOL-K) are the most sensitive parameters for the four stations, but the sensitivity of other parameters differs among these stations—for example, the third-order sensitive parameters at Dehkadeh Sefid (Sefid), Dehkadeh Sefid (Gavgodar), Chameriz and Dorudzan Dam are SOL-AWC, ALPHA-BF, GW-DELAY and GWQMN, respectively.

Water security assessment

GW security

The mean annual values of soil-water content over the watershed during the observation period (1981–2015) and three RCPs (2026–2085) are presented in Fig. 7. Soil-water content varies from 500 to 1560 mm/year during the observation period, resulting in a spatial-averaged value of 929 mm/year. The spatial-averaged soil-water content decreases from 929 mm/year in the present time to 891, 816 and 787 mm/year under RCP2.6, RCP4.5 and RCP8.5, respectively, corresponding to the percentage reductions of 4, 12.16 and 15.3%, respectively. Therefore, the available water for growing plants will decrease over the watershed. Climate change will also increase mean annual evapotranspiration over the region (Fig. 7). The spatial-averaged evapotranspiration will increase from 405 mm/year in the observation period (1981–2015) to

Fig. 6 Comparison between daily observed and simulated flow at four hydrometric stations during the calibration (1981–2005) and validation (2006–2015) periods



460, 465 and 470 mm/year under RCP2.6, RCP4.5 and RCP8.5, respectively, resulting in percentage change by +13.6, +14.8 and +16%, respectively. Reduced soil-water content associated with increased evapotranspiration under climate change will intensify green water scarcity and vulnerability in the future. The mean annual scarcity varies from 0.35 to 0.75 over the watershed during the observation period in which the spatial-averaged value is 0.47 (Fig. 7). The ranges of scarcity are 0.43–1.2, 0.46–1.35 and 0.5–1.36 under RCP2.6, RCP4.5 and RCP8.5, respectively, resulting in spatial-averaged values of 0.7, 0.76 and 0.78, respectively. The scarcity values greater than 1 indicate growing plants under water stress (soil-water deficit condition). Soil-water deficit may be compensated by the increase of irrigation depth supplied from the river water or groundwater abstraction. Therefore, crops' irrigation water requirements will increase under climate change. The water-stressed areas (scarcity >1) are located in regions where soil-water content is minimum relative to the remaining watershed areas (Fig. 7). The spatial distribution map of mean annual vulnerability is similar to that depicted for scarcity (Fig. 7). The ranges of vulnerability are 0.4–1.05, 0.45–1.33, 0.49–1.5 and 0.5–1.5 for the observation period, RCP2.6, RCP4.5 and RCP8.5, respectively,

corresponding to spatial-averaged values of 0.73, 0.78, 0.81 and 0.86, respectively. The watershed is generally not vulnerable to droughts now (except for negligible areas that cover about 2%), but climate change will increase the vulnerability such that about 13, 20 and 23% of the watershed will be vulnerable under the RCP2.6, RCP4.5 and RCP8.5, respectively.

Mean values of green water scarcity and vulnerability for each month during the observation and future periods are depicted in Figs. 8 and 9, respectively. Minimum scarcities and vulnerabilities occurred during winter (Dec–Jan–Feb) and maximum values during summer (Jun–Jul–Aug) for the observation period. The ranges of scarcity and vulnerability differ among the subbasins due to the variety of soil, land use and precipitation distribution inside each subbasin. However, no subbasin experiences green water scarcity and vulnerability during the observation period based on the mean annual values, but inter-annual analysis shows that the dominant subbasins experience green water stress (scarcity >1) at least during 1 month or during the whole summer. The irrigation depth must be increased during dry months to compensate the soil-water deficit in agricultural areas. The scarcity and vulnerability of green water will generally increase during all months

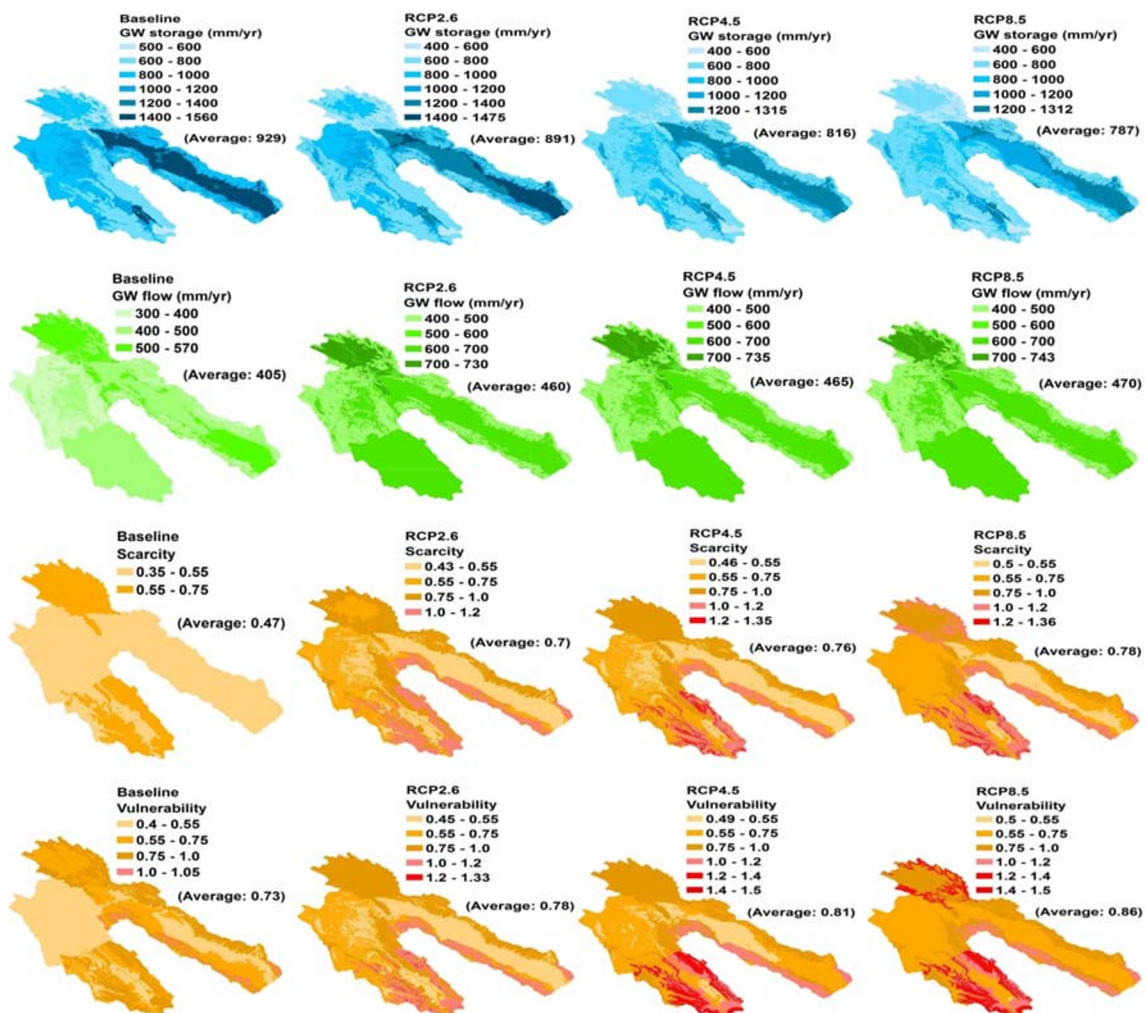


Fig. 7 Spatial distribution of mean annual green water (GW) storage, flow, scarcity and vulnerability during the observation period (1981–2015) and three RCPs (2026–2085)

under climate change due to reduced precipitation and increased temperature. Though high scarcity and vulnerability values are only in summer during the observation period, high values occur during summer (Jun–Jul–Aug) and 2 months in spring (Mar–Apr–May) under climate change. Green water scarcity and vulnerability values under climate change indicate that the irrigation depth must be increased during two seasons of spring and summer, even though high scarcity and vulnerability are observed only in summer during the observation period, to compensate the soil-water deficit in agricultural areas.

Surface blue-water security

The mean annual surface blue-water distribution under the present time and under climate change is depicted in Fig. 10. The spatial distribution of surface blue water is mainly affected by precipitation distribution over the watershed. The western and south-western regions that receive greater

precipitation have higher surface blue-water flow. The spatial-averaged surface blue-water flow is 227 mm/year over the watershed but it will reduce to 150, 145 and 146 mm/year under the RCP2.6, RCP4.5 and RCP8.5, respectively. The corresponding percentage reductions are 33.9, 36.1 and 35.7%, respectively. Climate change will substantially reduce available surface water for consumption in the future. Monthly abstraction rates from each subbasin of the Kor River at year 2009 are presented in Table 2 (Iranian Water Resources Management Company 2016). In this study, there were no further data sets of measured abstraction rates at different years and only the mentioned data set (for the year 2009) was available. Therefore, abstraction values of this data set are used in this research. Annual abstraction rate varies from zero to 2.6 m³/s among the subbasins. The abstracted river water is totally used for irrigation over the study area (Farsab Sanat Consulting Engineers 2010); therefore, the surface blue-water footprint at each subbasin is equal to the total volume (100%) of abstracted river water.

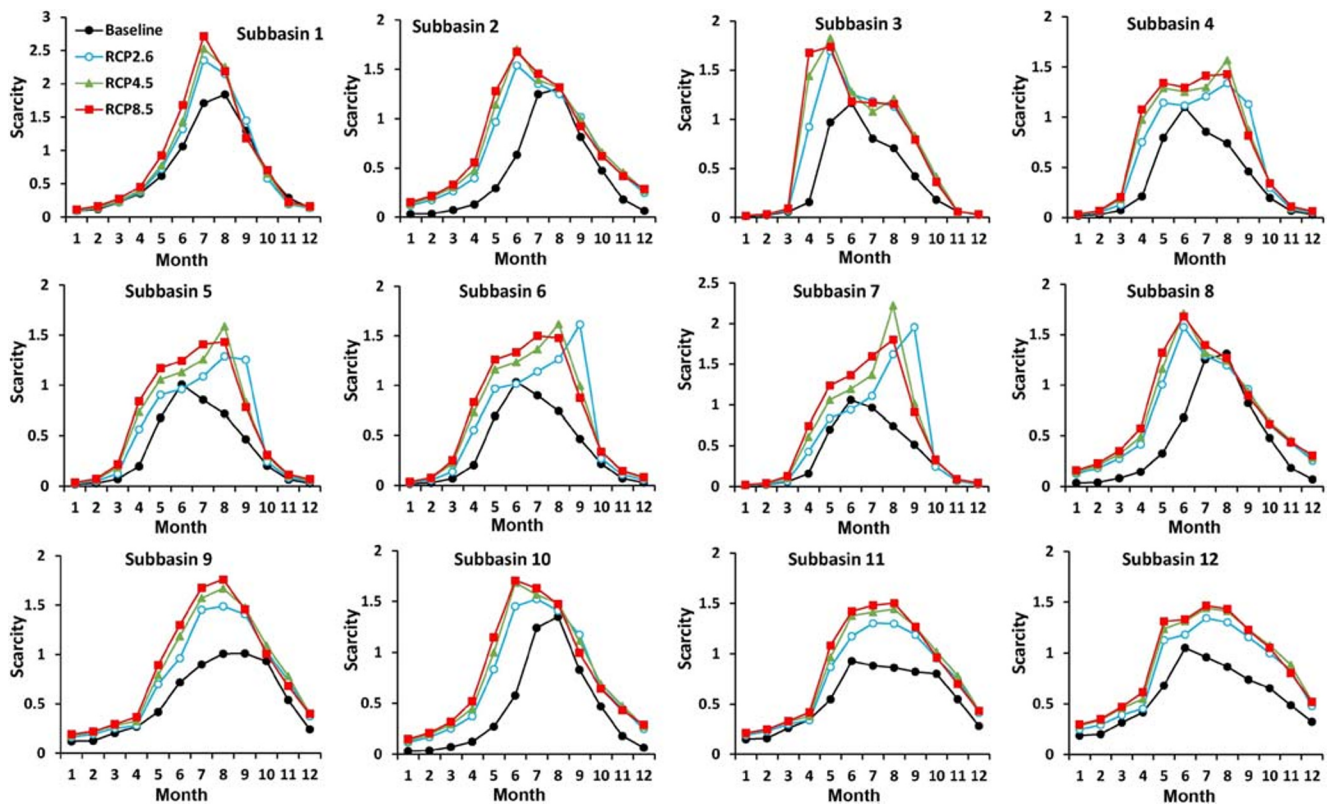


Fig. 8 Mean monthly scarcities of green water (GW) during the observation period and three RCPs

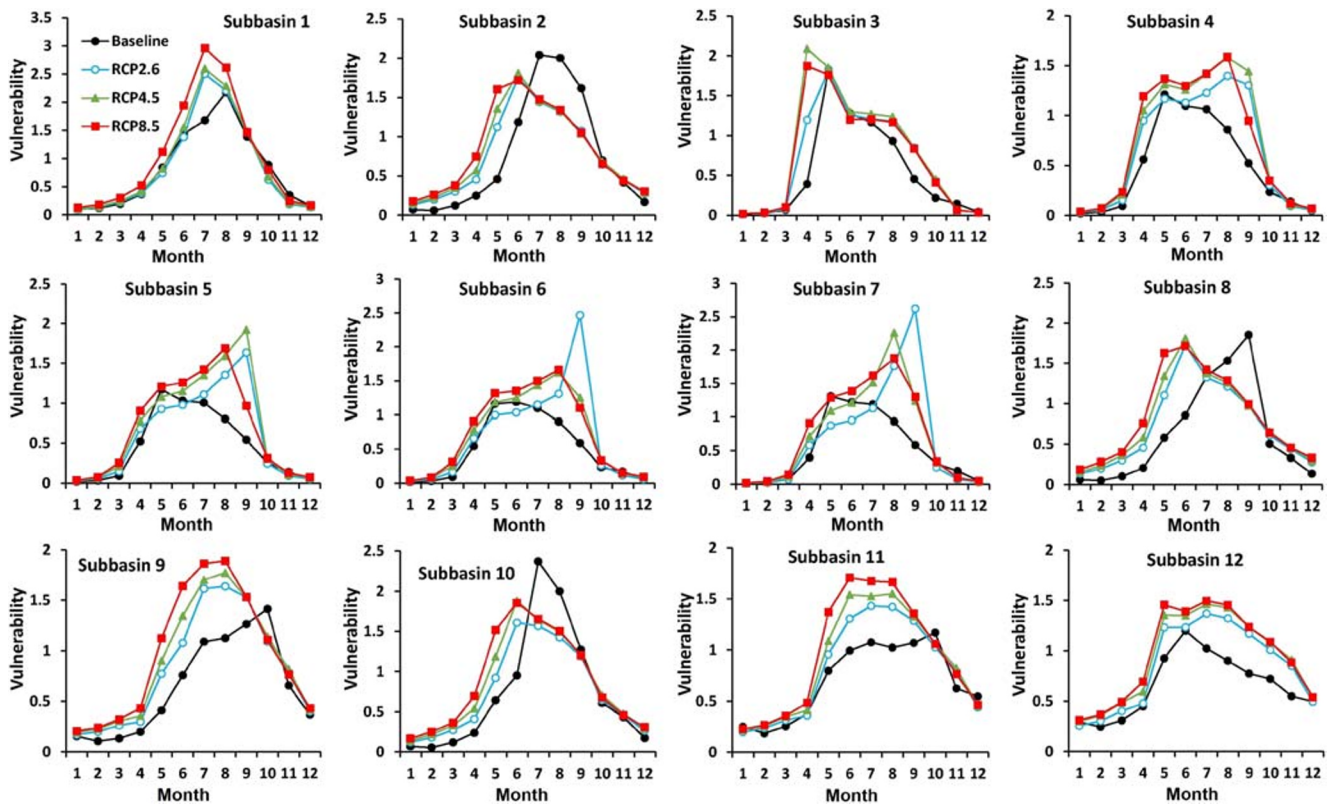


Fig. 9 Mean monthly vulnerabilities of green water (GW) during the observation period and three RCPs

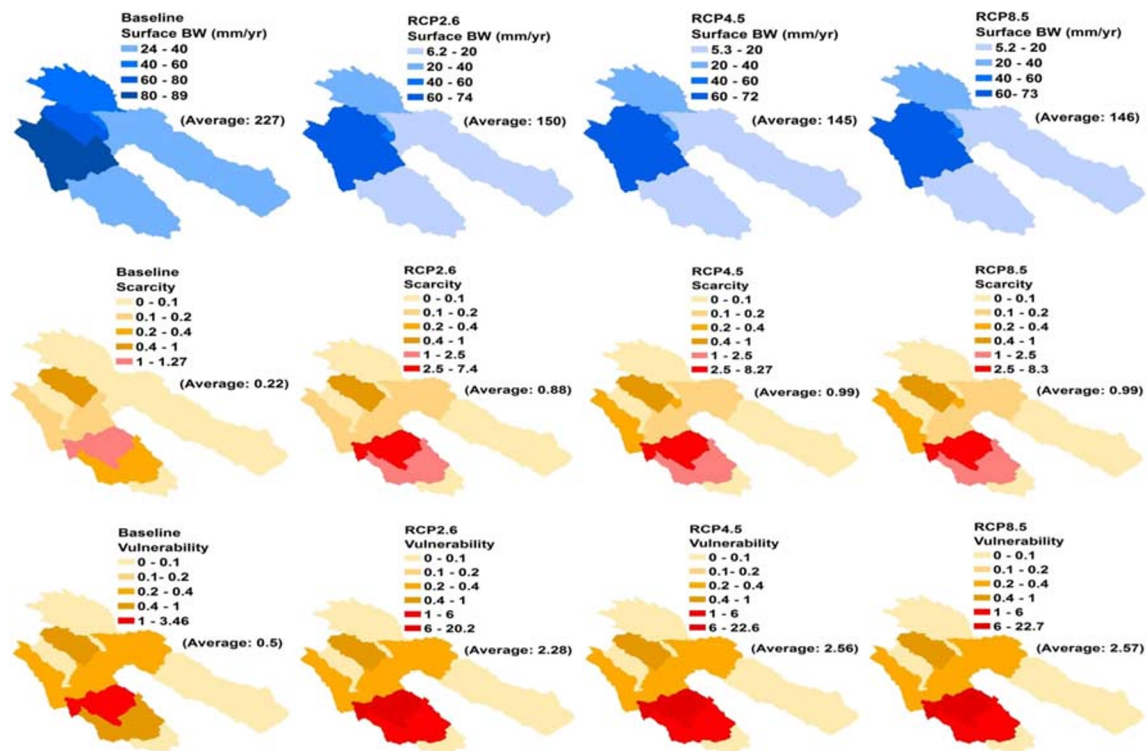


Fig. 10 Spatial distribution of mean annual surface blue water (surface BW), surface blue water scarcity and vulnerability during the observation period (1981–2015) and three RCPs (2026–2085)

Surface blue-water scarcity and vulnerability for each subbasin are calculated based on water consumption at the reference year 2009 under present time (1981–2015) and three RCPs (Fig. 10). The maximum scarcity value is 1.27 (subbasin 9) during the observation period; however, climate change will increase scarcity over the watershed such that maximum values are 7.4, 8.27 and 8.3 under the RCP2.6, RCP4.5 and RCP8.5, respectively. The subbasins with scarcity greater than 1 are referred to as “hotspots” where over-exploitation of river water leads to damage to the river-dependent ecology. The abstraction rate from the rivers must be reduced in hotspots to compensate for the effect of climate change in the future. Transportation of water from adjacent subbasins having no water stress (scarcity ≤ 1) is an alternative to supply water shortage in hotspots. Some regions (8.6% of the watershed) are vulnerable (>1) over the watershed during the observation period, but climate change will increase vulnerability such that about 19% of the watershed will be vulnerable under climate change (Fig. 10). Maximum vulnerability is 3.46 at the present time but it increases to 20.2, 22.6 and 22.7 under the RCP2.6, RCP4.5 and RCP8.5, respectively. Therefore, climate change will substantially increase vulnerability values over the watershed, leading to an increased number of ecological hotspots during droughts. One way to make the hotspots disappear under climate change is to reduce the future abstraction rate from rivers.

The mean values of surface blue-water scarcity and vulnerability for each month during the observation and future periods are depicted in Figs. 11 and 12. Security indices are presented for nine subbasins where river water is abstracted for consumption. Security indices for the remaining three subbasins are zero due to zero rate of water abstraction. The scarcity and vulnerability values are low in winter and spring, but increase and reach maximum during summer, then decreases gradually in autumn during the observation period; however, the level of scarcity and vulnerability varies among the subbasins due to different abstraction rates and available water. The scarcity and vulnerability of surface blue water increase dramatically in subbasins 9 and 11 under climate change (Figs. 11 and 12). The river-water abstraction is highest in these subbasins (Table 2) within the study area. On the other hand, climate change will reduce surface blue water within the study area in which reduction is higher in these two subbasins than the remaining subbasins. Consequently, the higher abstraction rate associated with the greatest blue-water reduction due to climate change will lead to a dramatic increase in security indices and raised ecological hotspots (see annual security indices in Fig. 10). Climate change will increase scarcity and vulnerability of surface blue water during all months such that the increase is greater for summer. Under climate change, subbasin 4 has scarcity and vulnerability values greater than 1 (referred as ecological hotspot) during the summer, while subbasins 9 and 11 have

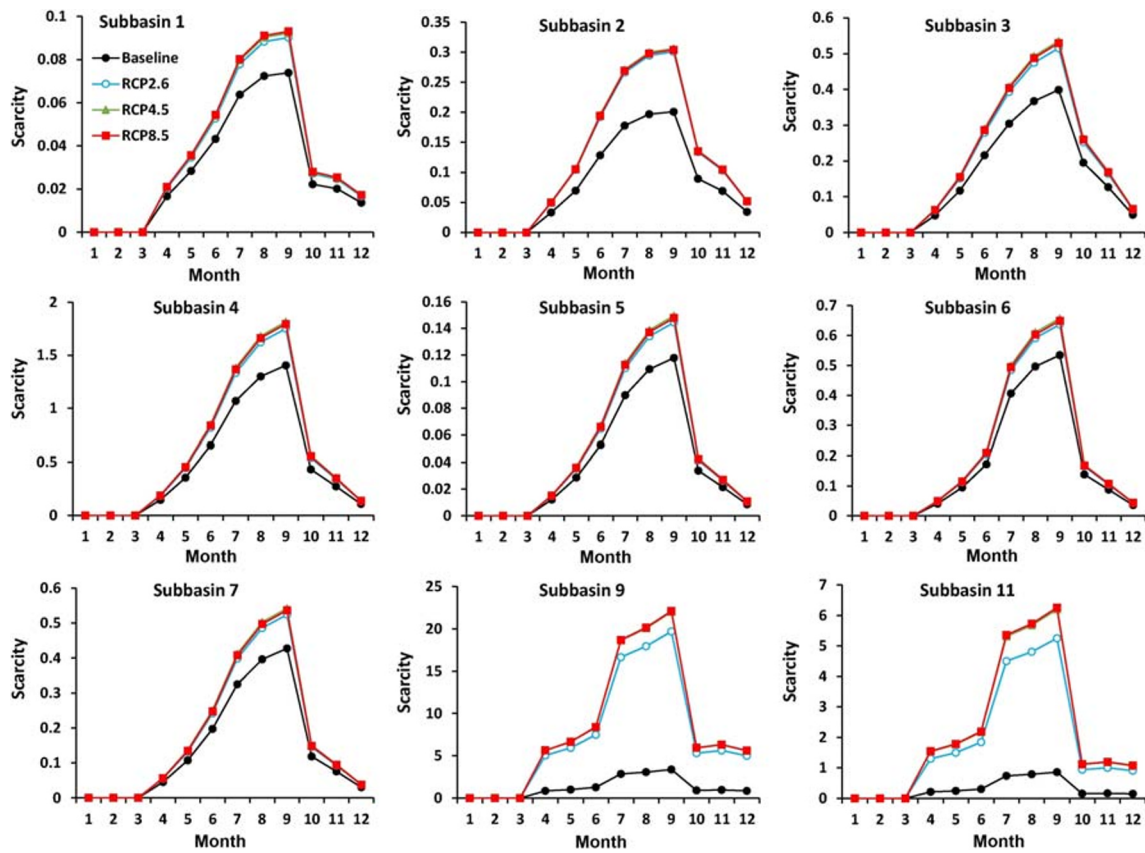


Fig. 11 Mean monthly scarcities of surface blue water during the observation period and three RCPs

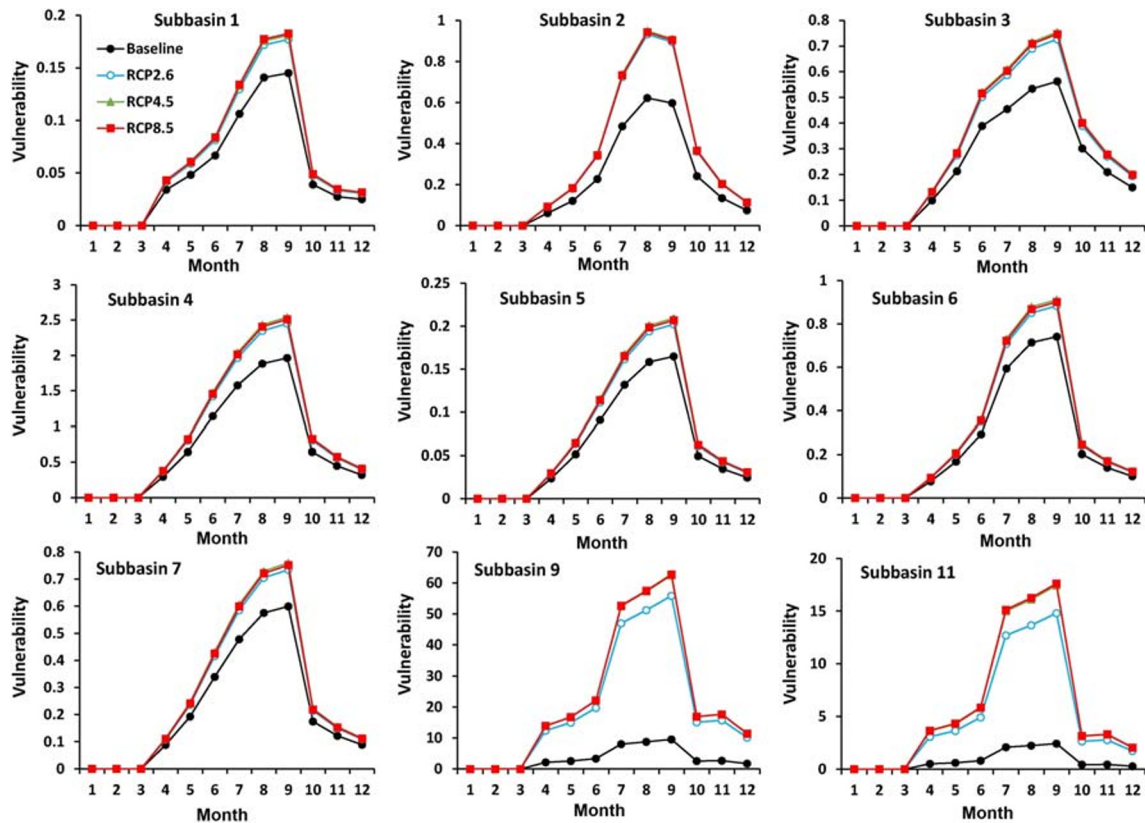


Fig. 12 Mean monthly vulnerabilities of surface blue water during the observation period and three RCPs

values greater than 1 during a period of 9 months (April–December). The remaining subbasins still have scarcity and vulnerability values less than 1 during all months. Response of water scarcity at each subbasin to climate change depends on the observed scarcity values and amount of available water in the future. The maximum scarcity and vulnerability values during the observation period and three RCPs occurred during summer and the first month of autumn.

Subsurface blue-water security

The spatial distribution map of mean annual subsurface blue water during the observation period and three RCPs is depicted in Fig. 13. Subsurface blue-water flow varies from 53 to 170 mm/year during the observation period in which the spatial-averaged value is 114 mm/year over the watershed. Climate change will substantially reduce the spatial-averaged subsurface blue-water value to 17, 13 and 12 mm/year under the RCP2.6, RCP4.5 and RCP8.5, respectively, corresponding to percentage reductions of 85, 88 and 89%, respectively.

Groundwater from the three alluvial aquifers Aspas, Khosroshirin and Kamfiruz (Fig. 13) are exploited for irrigation, municipal and industrial uses within the watershed. The mean annual groundwater exploitation rates ($\text{subBW}_{\text{footprint}}$ in Eq. 10) from Aspas, Khosroshirin and Kamfiruz are 190, 26.5 and 55.6 million cubic meter (MCM) during the period 2005–2015, respectively (Table 3), based on data provided by the

Iranian Water Resources Management Company (2016). Irrigation water is also supplied by additional river water abstraction and transportation of spring waters from adjacent karstic aquifers to the alluvial aquifers (Farsab Sanat Consulting Engineers 2010). Total additional supplied water for Aspas, Khosroshirin and Kamfiruz is 51.93, 8.45 and 115.44 MCM, respectively (Table 3); therefore, the total annual water supply for Aspas, Khosroshirin and Kamfiruz is 241.93, 34.95 and 171.04 MCM, respectively. The percentage water use in the agriculture and municipal-industrial sectors differs among the aquifers. The agricultural percentage uses vary from 57.6 to 88.75%, while municipal-industrial uses vary from 0.89 to 7.86% (Table 3). Recharge of the aquifers from municipal-industrial uses is 80% of water use in the three aquifers, while irrigation return flow varies from 20 to 27% throughout the aquifers (Table 3; Farsab Sanat Consulting Engineers 2010). Therefore, aquifer recharge from total water use (agriculture and municipal-industrial sectors) for Aspas, Khosroshirin and Kamfiruz is 55.13, 7.63 and 35.42 MCM, respectively (Table 3).

The mean annual groundwater scarcity and vulnerability are calculated for alluvial aquifers during the observation period (2005–2015) and three RCPs (2026–2085; Fig. 13). Scarcity in all aquifers is greater than 1 (1.37–1.65) during the observation period, indicating over-exploitation from the aquifers. Groundwater over-exploitation has been evidenced by dropped water tables in the three aquifers since 2000 (Iranian Water Resources Management Company 2016). The

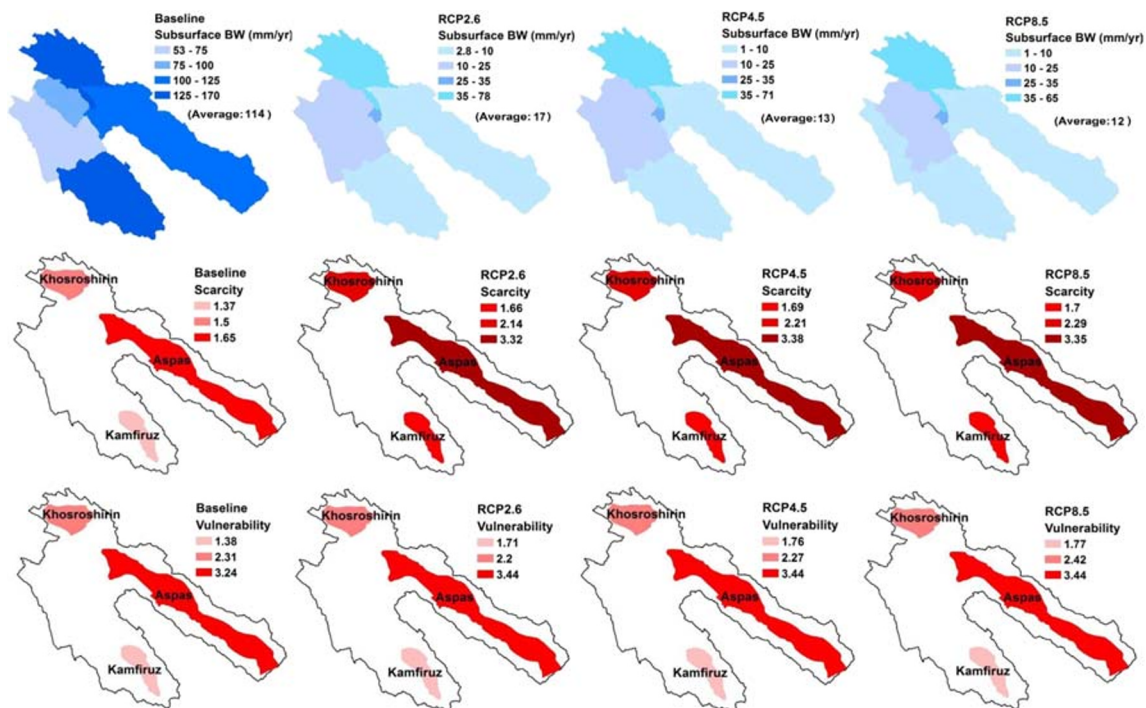


Fig. 13 Spatial distribution of mean annual subsurface blue water (subsurface BW), groundwater scarcity and vulnerability for the three alluvial aquifers during the observation period (2005–2015) and three RCPs (2026–2085)

Table 3 The annual groundwater exploitation, additional water supply, percentage water use in agricultural and municipal-industrial sectors, and groundwater recharge from water use data in three aquifers of the study area during the period 2005–2015

Parameter	Aspas	Khosroshirin	Kamfiruz
Groundwater exploitation (MCM/year)	190	26.5	55.6
Additional water supply from river (MCM/year)	2.7	2.6	97.67
Additional water supply from adjacent karstic springs (MCM/year)	49.23	5.85	17.77
Total additional water supply (MCM/year)	51.93	8.45	115.44
Total water supply (MCM/year)	241.93	34.95	171.04
Percentage use in agricultural sector	88.3	57.6	88.75
Percentage use in municipal-industrial sector	0.89	7.86	3.7
Water consumption in agricultural sector (MCM/year)	213.63	20.14	151.8
Water consumption in municipal-industrial sector (MCM/year)	2.15	2.74	6.32
Irrigation return flow (%)	25	27	20
Municipal-industrial return flow (%)	80	80	80
Recharge from irrigation (MCM/year)	53.4	5.43	30.36
Recharge from municipal-industrial water use (MCM/year)	1.72	2.2	5.06
Total recharge from water consumption (MCM/year)	55.13	7.63	35.42

present groundwater use from all aquifers is now very vulnerable during droughts. The Kamfiruz and Aspas aquifers have minimum (1.38) and maximum (3.24) vulnerabilities during the observation period (Fig. 13). Scarcity and vulnerability of the three aquifers will increase under climate change due to reduced precipitation and increased temperature (Fig. 13) in the future—for example, maximum groundwater scarcity will increase from 1.65 in the present time to 3.32, 3.38, and 3.35 under the RCP2.6, RCP4.5 and RCP8.5, respectively. Therefore, groundwater shortage will be intensified in the future due to climate change even with no increase in water demand.

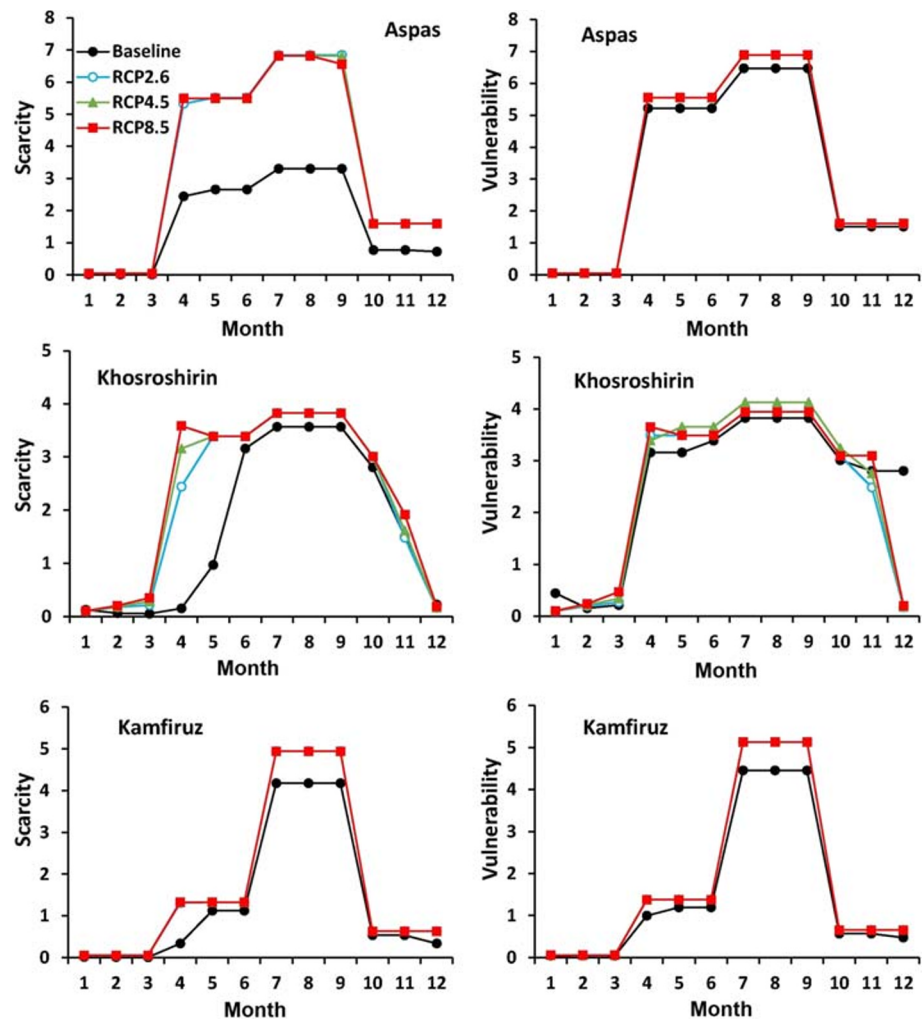
Mean monthly values of subsurface blue-water scarcity and vulnerability in the three aquifers are presented in Fig. 14. Security indices (scarcity and vulnerability) for the three aquifers are minimum in January, February and March, while they are maximum in summer during the observation period. The observed scarcities are generally less than 1 in all aquifers (except in Khosroshirin) for 6 months (Jan, Feb, Mar, Oct, Nov, Dec) and greater than 1 for the remaining months of the year, indicating that groundwater abstraction is not sustainable (>1) during these months due to groundwater storage depletion. Climate change will increase scarcity values such that the groundwater abstraction is not sustainable during most times of the year, except in winter, due to limited groundwater availability in the future. The response of vulnerabilities to climate change in the three aquifers is similar to that for scarcity values, indicating that groundwater abstraction will be more vulnerable to droughts under climate change. The vulnerability values under RCP4.5 for certain months are slightly higher than those of RCP8.5 in Khosroshirin aquifer (Fig. 14). Groundwater recharge during droughts for these months of RCP4.5 is slightly lower than those of RCP8.5, leading to lower availability of groundwater and higher vulnerability in

this aquifer. Groundwater recharge depends on the precipitation depth, soil bulk density, soil field capacity and thickness, type of land use and evapotranspiration. The result of the response of these components to climate change finally determine groundwater recharge rate.

Vulnerability relates water footprint to low volume of available water (represented as 30th percentile of available water) at normal periods. In other words, vulnerability is the scarcity of water during dry periods when available water for consumption is less than available water at normal periods. Vulnerability of the three aquifers is near the scarcity values in January, February and March, but it is greater in remaining months. This implies that during wet months there is low availability of groundwater during droughts, but this availability increases during normal periods; therefore, groundwater recharge during the wet months of dry years is near the recharge during wet months of normal years (precipitation is still high enough to recharge groundwater during wet months of a drought). Higher vulnerability values in remaining months, especially in summer, indicate that the groundwater recharge, and subsequently available groundwater, significantly reduces during droughts comparing to the normal periods. Lower availability of groundwater during dry months of a drought may be due to greater reduction of soil-water content comparing to reduced soil-water content during dry months of a normal year. When soil-water content is depleted, a smaller fraction of precipitation moves downward to finally recharge the aquifer.

The mean annual water balance components over the watershed are presented in Table 4. Fifty-four percent of the precipitation (751 mm/year) is returned to the atmosphere via evapotranspiration (405 mm/year), 0.66% stored in the soil (5 mm/year), 36.64% percolates (275.17 mm/year) and 8.7% contributes to the surface flow (65.83 mm/year) during the

Fig. 14 Mean monthly scarcities and vulnerabilities of subsurface blue water during the observation period and three RCPs



observation period. Climate change disturbs this partitioning such that a greater fraction of precipitation (70–74.6%) is returned to the atmosphere via evapotranspiration under different RCPs (460–470 mm/year). The fractions of stored precipitation in soil, percolation and contribution to surface flow also will decrease under climate change. For example, the percolation fraction will decrease from 36.6% (275.17 mm/year) at the present time to 17% (107.25 mm/year) in the future, and/or the share of precipitation in the surface flow will decrease from 8.7% (65.83 mm/year) to 7.6% (49.5 mm/year) under climate change. The available green water (initial soil-water content) will also decrease from 929 mm/year at the present time to 787 mm/year in the future. The long-term percolated water (water that moves downward from the root zone to reach the shallow water table) equals the long-term total groundwater recharges due to negligible water storage in the soil profile (Neitsch et al. 2011). However, these values are also identical in the HRU output for the long-term period. Recharge of the deep aquifer decreases from 5.2 mm/year during the observation period to 1.5, 0.1 and 0.15 mm/year under RCP2.6, RCP4.5 and RCP8.5, respectively, while

the shallow aquifer recharge changes from 270 mm/year to 116, 107.15 and 108.5 mm/year under the three RCPs, respectively. The baseflow will also decrease from 161 mm/year to 94.25 mm/year under climate change due to decreased shallow aquifer recharge. Precipitation contribution to the surface blue water (WYLD-Q) is 30% (227 mm/year) at the present time but it reduces to 23% (145 mm/year) in the future. Precipitation contribution to subsurface blue water (GW_RCHG minus GW_Q) is 15.2% (114 mm/year) at the present time and it reduces to 1.95% (12.3 mm/year) under climate change. Overall, it can be concluded that the precipitation reduction and temperature enhancement due to climate change will increase evapotranspiration, but decrease the soil-water content and the available surface and subsurface blue waters in the study area.

Discussion

In this report, groundwater security in three aquifers are evaluated using the results provided by the SWAT. The scarcity

Table 4 The mean annual water balance components (mm/year) over the watershed during the observation period and three RCPs

Component	Period			
	Observation (1981–2015)	Future (2026–2085)		
		RCP2.6	RCP4.5	RCP8.5
Precipitation (PRECIP)	751	653	624	630
Green water flow (ET)	405	460	465	470
Green water storage (SW _{initial})	929	891	816	787
Change in soil-water content (Δ SW)	5	26	1	1.7
Final soil-water content (SW _{final})	934	917	817	788.7
Percolation (PERC)	275.17	117.5	107.25	108.66
Lateral and surface discharge (LATQ + SURQ)	65.83	49.5	50.75	49.64
Total groundwater recharge (GW_RCHG)	275.17	117.5	107.25	108.66
Deep aquifer recharge (DA_RCHG)	5.2	1.5	0.1	0.15
Shallow aquifer recharge (SA_RCHG)	269.97	116	107.15	108.51
Water in shallow aquifer returning to the root zone (REVAP)	15.2	12.3	10.7	11.5
Baseflow (GW_Q)	161.17	100.5	94.25	96.36
Change in shallow aquifer storage (Δ SA_ST)	93.6	3.2	2.2	0.65
Surfaceblue water (WYLD_Q)	227	150	145	146
Subsurface blue water (GW_RCHG) - (GW_Q)	114	17	13	12.3

relates to available groundwater storage defined as total groundwater recharge (recharge from precipitation and water uses) minus river baseflow. The term “available groundwater storage” used in this study shows mean annual volume of renewable groundwater which is available for human consumption. Renewable groundwater storage is the portion of groundwater that can be recharged and replaced annually (dynamic storage) and it does not include the static storage. Static storage is the main portion of the aquifer storage that cannot be recovered annually and a long period is required for recovery. Therefore, when scarcity is higher than 1, a portion of abstracted water originates from static storage, leading to groundwater depletion and water-table drop. To validate the results, SWAT-modeled available groundwater storage is compared to that calculated using the water balance approach presented by Farsab Sanat Consulting Engineers (2010). There is extensive agricultural area over the watershed where farmers irrigate different crops by different irrigation systems, timings

and management schemes. There were no data for accurate irrigation planning and design in SWAT; however, it would have been difficult to include these factors even if data were available. Therefore, no irrigation planning was included in the SWAT model and, instead, the groundwater recharge from irrigation and municipal-industrial uses were calculated using data provided by Farsab Sanat Consulting Engineers (2010; see Table 3). The SWAT-calculated groundwater recharge from precipitation for Aspas, Khosroshirin and Kamfiruz are 99.4, 27.8 and 25.6 MCM, respectively and the corresponding values calculated using the water balance approach (Farsab Sanat Consulting Engineers 2010) are 118.1, 32.44, 28.32 MCM, respectively. The water balance approach ignores the variation of soil-moisture content as a component of water balance and consequently it estimates the potential groundwater recharge; however, SWAT-estimated values present actual recharge. Therefore, SWAT-estimated values (smaller values) seem to be reliable. For more sound results, the consistency

between values of scarcity and groundwater depletion in the three aquifers is provided during the observation period. The mean annual values of scarcity for Aspas, Khosroshirin and Kamfiruz aquifers are 1.65, 1.5 and 1.37 (Fig. 13), respectively, while the mean annual depletion of groundwater storage (static storage) values are 26.16, 5.07 and 1.27 MCM, respectively (Iranian Water Resources Management Company 2016). This indicates that greater scarcity values are associated with larger groundwater depletion over the region.

Abbaspour et al. (2009) studied the impact of climate change on blue and green water resources in Iran. They found that evapotranspiration will increase under climate change. Blue water for the period 2073–2099 relative to 1980–2002 will increase by 25 and 50% in scenarios B1 and A2, respectively but it will decrease by 10% in the intermediate scenario A1B. In their study, only one hydrometric station was used in the study area to calibrate the SWAT values based on monthly river flows. Climate change was studied using output of only one GCM under the old scenarios B1, A1B and A2. They did not present any results for the groundwater recharge and storage, and also they did not present any security assessment for the study area. In this research, the SWAT is calibrated using daily discharge data measured at four hydrometric stations to assess the security of green water resources and surface and subsurface blue water resources under the present time and under climate change. Climate change over the region is studied using outputs of 22 GCMs, instead of one GCM, under new scenarios RCP2.6, RCP4.5 and RCP8.5.

Faramarzi et al. (2009) used the SWAT to assess blue and green water resources in Iran where the hydrological model was calibrated using monthly discharge data measured at two hydrometric stations within the study area. The mean annual values of blue water and actual evapotranspiration for the period of 1990–2002 were estimated to be 300 and 475 mm/year, respectively (Faramarzi et al. 2009) over the study area; however, in this study, the corresponding values for the period 1981–2015 are estimated to be 341 and 405 mm/year, respectively. They did not present any security assessment of water resources for the study area.

Climate-change study over the watershed of Dorudzan Dam reveals that the temperature change is consistent with the level of warming of RCPs where minimum and maximum increase of temperature are in the RCP2.6 and RCP8.5 scenarios, respectively. However projected precipitation does not show a consistency with level of warming because minimum and maximum precipitation reductions are in the RCP2.6 and RCP4.5 scenarios (instead of RCP8.5), respectively. Precipitation projection under climate change in different regions show that there may be no consistency between precipitation change and temperature anomaly—for example, precipitation over the watershed of Karaj-Jajrud in Iran will decrease by 5, 9 and 4.7% under RCP2.6, RCP4.5 and RCP8.5,

respectively (Mirdashtvan et al. 2018). Precipitation in south-eastern Iran decreases by 12.5% in RCP4.5 but it increases by 20% in RCP8.5 (Vaghefi et al. 2019). Precipitation in India for the period of 2046–2075 relative to 1861–1900 will decrease by 2.7, 4.3, 3.5 and 6.6% under RCP2.6, RCP4.5, RCP6 and RCP8.5, respectively (Chaturvedi et al. 2012), whereas precipitation in the Xin River Basin of China increases by 6, 4 and 14% under RCP2.6, RCP4.5 and RCP8.5, respectively (Zhang et al. 2016). Climate change studies in the Middle East region show that raised temperature under climate change increases evaporation from water bodies (oceans and lakes) and leads to increased absolute humidity of the air parcel (Evans 2010; Mariotti et al. 2008). Climate change warms both land masses and water bodies; however, the increase of temperature over land is higher than that of oceans and lakes (Evans 2010; Mariotti et al. 2008), making the temperature lapse rate change over them. The contrast in warming over land and water bodies associated with changed temperature lapse rate leads to an upward shift of the condensation level of the air parcel (O’Gorman and Schneider 2009; O’Gorman 2015; Siler and Roe 2014; Singh and Goyal 2016). Increased absolute humidity of the air has a potential to produce high precipitation amounts if it is triggered by an external mechanism such as lifting forced by topography (Evans 2010). The complexity of processes (relative and absolute humidity of the air, land temperature lapse rate, air condensation level, land and ocean warming contrast, wind velocity and direction, surface albedo) that produce orographic precipitation and different responses of each process to climate change lead to inconsistency between the level of warming and precipitation change in the region. Climate change over the watershed of Dorudzan Dam is studied using statistical downscaling for impact assessment; however, to understand physical-based mechanisms of precipitation reduction in this region, a dynamic downscaling is recommended.

Conclusion

In this study, the water security (scarcity and vulnerability) of blue and green water resources is assessed for the large watershed of Dorudzan Dam in northern Fars Province of southern Iran, under present time and three climate change scenarios (RCP2.6, RCP4.5, RCP8.5). Mean annual precipitation will decrease (13–17%), while mean annual temperature will increase (+1.7 to +3.3 °C) under the three RCPs. A reduced dam inflow by about 50% in the future will lead to limited availability of water in downstream areas and intensified water shortage under climate change.

Mean annual evapotranspiration will increase (13.6–16%) while soil-water content will decrease (4–15.3%) under the three RCPs. Climate change will increase green water scarcity and vulnerability over the watershed. The irrigation water

requirement will also increase due to increased evapotranspiration and reduced soil-water content. Monthly scarcity values for the observation period show that dominant subbasins experience green water stress (scarcity >1) at least during 1 month or during the entire summer, but they experience the water stress during two seasons of spring and summer under climate change. Therefore, irrigation depth must be increased during spring and summer, even though high scarcity and vulnerability are observed only in summer during the observation period, to compensate the soil-water deficit in agricultural areas.

Mean annual security values of surface blue water show one ecological hotspot (subbasin 9) over the watershed during the observation period, but climate change will increase scarcity and vulnerability values such that two ecological hotspots (subbasins 9 and 11) will appear. Monthly security indices show that scarcity and vulnerability values are minimum in winter and maximum in summer at the present time and in the future. Climate change will increase scarcity and vulnerability values during all months (increase is higher for dry season, i.e., summer). Maximum scarcity and vulnerability values during the observation period and the three RCPs occur during summer.

Groundwater exploitation is not sustainable in the three aquifers (evident by water-table decline) during the observation period; however, reduced availability of groundwater in the future will intensify the water crisis in this region. Monthly security indices for the observation period reveal that scarcity values are minimum during winter and maximum in summer and autumn. Groundwater abstraction is only sustainable in 6 months of the year during the observation period; however, climate change will increase the scarcity values such that groundwater abstraction is not sustainable during much of the year due to limited groundwater availability in the future.

The results of this study indicate that climate change has the potential to affect water security in the region. However, the response of each water balance component to climate change is not identical—for example, maximum green water and surface blue water scarcities occurred during summer, while subsurface-blue-water-maximum scarcity was during most of the year. Climate change may increase or decrease water scarcity, depending on the projected precipitation and temperature under climate change. In regions, such as that in this study, where climate change will increase water scarcity, reoriented management alternatives are required for sustainable development. Abstraction rate must be reduced in those surface water and groundwaters that are under water stress (scarcity >1) to compensate for the effect of climate change. Management alternatives for abstraction reduction in a region may include: cultivated-area reduction, irrigation-efficiency enhancement, using treated industry effluent for irrigation, shifting cropping patterns (e.g. planting crops with low

irrigation requirement instead of crops with high irrigation requirement) and inter-basin water allocation and transportation.

Acknowledgements The author acknowledges the World Climate Research Programme's Working Group on Coupled Modelling, which is responsible for CMIP5, and the climate modeling groups for producing and making available their model output. Help from the Iran Water Resources Management Company in providing the local data is greatly appreciated. The author declares that he has no conflicts of interest.

Funding information The author is thankful for support from the Institute for Advanced Studies in Basic Sciences in Zanjan, Iran.

References

- Abbaspour KC, Faramarzi M, Seyed Ghasemi S, Yang H (2009) Assessing the impact of climate change on water resources in Iran. *Water Resour Res* 45:1–16. <https://doi.org/10.2113/3.4.1340>
- Alijani B, Harman JR (1985) Synoptic climatology of precipitation in Iran. *Ann Assoc Am Geogr* 75:404–416. <https://doi.org/10.1111/j.1467-8306.1985.tb00075.x>
- Beyglou M, Khoshakhlagh F, Ovji R (2009) The seasonal location and frequency of cyclone tracks of wet periods in middle-western Iran. *Natl Geogr Res* 68:71–84. <https://doi.org/10.1007/s11069-015-1862-z>
- Chaturvedi RK, Joshi J, Jayaraman M, Bala G, Ravindranath N (2012) Multi-model climate change projections for India under representative concentration pathways. *Curr Sci* 103:791–802
- Chen J, Brissette FP, Leconte R (2011) Uncertainty of downscaling method in quantifying the impact of climate change on hydrology. *J Hydrol* 401:190–202
- Esnault L et al (2014) Linking groundwater use and stress to specific crops using the groundwater footprint in the Central Valley and High Plains aquifer systems, U.S. *Water Resour Res* 50:4953–4973
- Evans JP (2008) Changes in water vapor transport and the production of precipitation in the eastern fertile crescent as a result of global warming. *J Hydrometeorol* 9:1390–1401
- Evans JP (2010) Global warming impact on the dominant precipitation processes in the Middle East. *Theor Appl Climatol* 99:389
- Evans JP, Alsamawi A (2011) The importance of the Zagros Mountains barrier jet to future precipitation in the Fertile Crescent. *Open Atmos Sci J* 5:87–95
- Falkenmark M, Rockström J (2006) The new blue and green water paradigm: breaking new ground for water resources planning and management. *J Water Resour Plan Manag* 132:129–132. [https://doi.org/10.1061/\(ASCE\)0733-9496\(2006\)132:3\(129\)](https://doi.org/10.1061/(ASCE)0733-9496(2006)132:3(129))
- FAO/IIASA/ISRIC/ISSCAS/JRC (2009) Harmonized world soil database (version 1.1). FAO Rome, Italy and IIASA, Laxenburg, Austria
- Faramarzi M, Abbaspour KC, Schulin R, Yang H (2009) Modelling blue and green water resources availability in Iran. *Hydrol Proc* 23:486–501
- Farsab Sanat Consulting Eng. (2010) Studing the water resources over watershed of Tashk-Bakhtegan and Maharlou lakes: reports on water budget in Aspas, Khosroshirin and Kamfiruz plains (in Persian). Fars Regional Water Authority, Fars, Iran
- Giorgi F, Lionello P (2008) Climate change projections for the Mediterranean region. *Glob Planet Chang* 63:90–104
- Gleeson T, Wada Y (2013) Assessing regional groundwater stress for nations using multiple data sources with the groundwater footprint. *Environ Res Lett* 8:044010

- Ho JT, Thompson JR, Brierley C (2016) Projections of hydrology in the Tocantins-Araguaia Basin, Brazil: uncertainty assessment using the CMIP5 ensemble. *Hydrol Sci J* 61:551–567
- Hoekstra AY, Chapagain AK, Aldaya MM, Mekonnen MM (2011) The water footprint assessment manual: setting the global standard. Routledge, Abingdon, UK
- Iizumi T, Semenov MA, Nishimori M, Ishigooka Y, Kuwagata T (2012) ELPIS-JP: a dataset of local-scale daily climate change scenarios for Japan. *Philosophical Transactions Series A. Math Phys Eng Sci* 370: 1121–1139. <https://doi.org/10.1098/rsta.2011.0305>
- Iranian Water Resources Management Company (2016) Data center. <http://wrbs.wrm.ir>. Accessed 13 April 2020
- Knisel W, Sheridan J (1983) Procedure for characterizing hydrologic processes in the coastal plain of the southeastern United States proceedings hydrology on large flat lands. UNESCO International Programme on Hydrology, Paris
- Knutti R, Sedláček J (2013) Robustness and uncertainties in the new CMIP5 climate model projections nature. *Clim Change* 3:369
- Kourgialas NN, Karatzas GP, Dokou Z, Kokorogiannis A (2018) Groundwater footprint methodology as policy tool for balancing water needs (agriculture & tourism) in water scarce islands: the case of Crete, Greece. *Sci Total Environ* 615:381–389. <https://doi.org/10.1016/j.scitotenv.2017.09.308>
- Linsley Jr RK, Kohler MA, Paulhus JL (1975) Hydrology for engineers. McGraw-Hill, New York
- Lutz AF, ter Maat HW, Biemans H, Shrestha AB, Wester P, Immerzeel WW (2016) Selecting representative climate models for climate change impact studies: an advanced envelope-based selection approach. *Int J Climatol* 36:3988–4005
- Mariotti A, Zeng N, Yoon J-H, Artale V, Navarra A, Alpert P, Li LZ (2008) Mediterranean water cycle changes: transition to drier 21st century conditions in observations and CMIP3 simulations. *Environ Res Lett* 3:044001
- Mirdashtvan M, Najafinejad A, Malekian A, Sa’oddin A (2018) Downscaling the contribution to uncertainty in climate-change assessments: representative concentration pathway (RCP) scenarios for the South Alborz Range. *Iran Meteorol Appl* 25:414–422
- Mishra AK, Singh VP (2010) A review of drought concepts. *J Hydrol* 391:202–216. <https://doi.org/10.1016/j.jhydrol.2010.07.012>
- Naderi M, Raeisi E (2016) Climate change in a region with altitude differences and with precipitation from various sources, South-Central Iran. *Theor Appl Climatol* 124:529–540
- Naderi M, Saatsaz M (2019) Impact of climate change on the hydrology and water salinity in the Anzali wetland, northern Iran. *Hydrol Sci J*. <https://doi.org/10.1080/02626667.2019.1704761>
- Neitsch SL, Arnold JG, Kiniry JR, Williams JR (2011) Soil and water assessment tool theoretical documentation version 2009. Texas Water Resources Institute, College Station, TX
- O’Gorman PA (2015) Precipitation extremes under climate change. *Curr Clim Chang Rep* 1:49–59
- O’Gorman PA, Schneider T (2009) The physical basis for increases in precipitation extremes in simulations of 21st-century climate change. *Proc Natl Acad Sci* 106:14773–14777
- Papadopolou MP, Charchousi D, Tsoukala VK, Giannakopoulos C, Petrakis M (2016) Water footprint assessment considering climate change effects on future agricultural production in Mediterranean region. *Desalin Water Treat* 57:2232–2242. <https://doi.org/10.1080/19443994.2015.1049408>
- Richter BD, Davis MM, Apse C, Konrad C (2012) A presumptive standard for environmental flow protection. *River Res Appl* 28:1312–1321. <https://doi.org/10.1002/rra.1511>
- Rodrigues DBB, Gupta HV, Mendiondo EM (2014) A blue/green water-based accounting framework for assessment of water security. *Water Resour Res* 50:7187–7205. <https://doi.org/10.1002/2013WR014274>
- Roshani A, Parak F, Hejazizade Z, Ghaemi H (2013) Studying the moisture flux over south and southwest of Iran: a case study from December 10 to 13, 1995 rain storm. *Earth Sci Res J* 2:34–39. <https://doi.org/10.1007/s11069-015-1862-z>
- Rutledge AT (2007) Program user guide for PART. <https://water.usgs.gov/ogw/part/UserManualPART.pdf>. Accessed April 2020
- Semenov MA, Barrow EM (2002) LARS-WG: a stochastic weather generator for use in climate impact studies. <http://resources.rothamsted.ac.uk/sites/default/files/groups/mas-models/download/LARS-WG-Manual.pdf>. Accessed April 2020
- Semenov MA, Stratonovitch P (2015) Adapting wheat ideotypes for climate change: accounting for uncertainties in CMIP5 climate projections. *Clim Res* 65:123–139
- Shirmohammadi A, Knisel W, Sheridan J (1984) An approximate method for partitioning daily streamflow data. *J Hydrol* 74:335–354
- Siler N, Roe G (2014) How will orographic precipitation respond to surface warming? An idealized thermodynamic perspective. *Geophys Res Lett* 41:2606–2613
- Singh V, Goyal MK (2016) Analysis and trends of precipitation lapse rate and extreme indices over North Sikkim eastern Himalayas under CMIP5ESM-2M RCPs experiments. *Atmos Res* 167:34–60
- Thompson JR, Crawley A, Kingston DG (2017) Future river flows and flood extent in the upper Niger and inner Niger Delta: GCM-related uncertainty using the CMIP5 ensemble. *Hydrol Sci J* 62:2239–2265
- Ulbrich U, May W, Li L, Lionello P, Pinto JG, Somot S (2006) The Mediterranean climate change under global warming. *Develop Earth Environ Sci* 4:399–415
- Vaghefi SA, Keykhai M, Jahanbakhshi F, Sheikholeslami J, Ahmadi A, Yang H, Abbaspour KC (2019) The future of extreme climate in Iran. *Sci Rep* 9:1464
- Veetil AV, Mishra AK (2016) Water security assessment using blue and green water footprint concepts. *J Hydrol* 542:589–602. <https://doi.org/10.1016/j.jhydrol.2016.09.032>
- Winchell M, Srinivasan R, Di Luzio M, Arnold J (2013) ArcSWAT interface for SWAT2012: user’s guide. Grassland Soil and Water Research Laboratory, Temple, TX
- Zhang Y, Huang K, Yu Y, Hu T, Wei J (2015) Impact of climate change and drought regime on water footprint of crop production: the case of Lake Dianchi Basin. *Chin Nat Hazards* 79:549–566. <https://doi.org/10.1007/s11069-015-1862-z>
- Zhang Y, You Q, Chen C, Ge J (2016) Impacts of climate change on streamflows under RCP scenarios: a case study in Xin River basin. *Chin Atmos Res* 178:521–534